

# Resource Bounds for Quantum Circuit Mapping via Quantum Circuit Complexity

Matthew Steinberg<sup>1,2\*</sup>, Medina Bandić<sup>1,2\*</sup>, Sacha Szkuclarek<sup>1</sup>, Carmen G. Almudever<sup>3</sup>, Aritra Sarkar<sup>1,2</sup>, and Sebastian Feld<sup>1,2</sup>

<sup>1</sup>*Quantum Computing Division, QuTech, Delft University of Technology, Delft, the Netherlands*

<sup>2</sup>*Department of Quantum & Computer Engineering, Delft University of Technology, Delft, the Netherlands and*

<sup>3</sup>*Computer Engineering Department, Technical University of Valencia, Valencia, Spain*

(Dated: February 2, 2024)

Efficiently mapping quantum circuits onto hardware is an integral part of the quantum compilation process, wherein a quantum circuit is modified in accordance with the typically stringent architectural demands of a quantum processor. Many techniques exist for solving the quantum circuit mapping problem, in addition to several theoretical perspectives that relate quantum circuit mapping to problems in classical computer science. This work considers a novel perspective on quantum circuit mapping, in which the routing process of a simplified circuit is viewed as a composition of quantum operations acting on density matrices representing the quantum circuit and processor. Drawing on insight from recent advances in quantum resource theory, circuit complexity, and information geometry, we show that a minimal SWAP gate count for executing a quantum circuit on a device emerges via the minimization of the distance between quantum states using the quantum Jensen-Shannon divergence. Additionally, we develop a novel initial placement algorithm based on a graph similarity search that selects the partition nearest to a graph isomorphism between interaction and coupling graphs. From these two ingredients, we then construct a polynomial-time algorithm for calculating the SWAP gate lower bound, which is directly compared alongside the IBM Qiskit compiler for over 600 realistic benchmark experiments, as well as against a brute-force method for smaller benchmarks. In our simulations, we unambiguously find that neither the brute-force method nor the Qiskit compiler surpass our bound, implying utility as a precise estimation of minimal overhead when realizing quantum algorithms on constrained quantum hardware. This work constitutes the first use of quantum circuit uncomplexity to practically-relevant quantum computing. We anticipate that this method may have diverse applicability outside of the scope of quantum information science, and we discuss several of these possibilities.

## I. INTRODUCTION

The promise of quantum technology extends to many areas of modern theoretical physics, computer science and cryptography, among others [1]. In spite of much success over the past 30 years, current-generation quantum technology is characterized by noisy, intermediate-scale devices that are severely limited not only by the depth and size of the quantum circuits that can be executed, but also by the qubit connectivity of such devices [2]. Such processors, have allowed for the first generation of quantum-technology demonstrations, ranging from experimental realizations of hybrid quantum-classical optimization techniques [3, 4] to resource-intensive algorithms such as fault-tolerant quantum error-correction codes (QECCs) [5–7].

With such promise as is forecasted for quantum technology, *full-stack* design approaches have emerged, in order to delegate resources efficiently and to ensure high success rates for a given quantum circuit, realized on a quantum processor [8–10]. As such, one of the cardinal issues to emerge for practical quantum computing is that of *quantum compilation*, which can be broadly defined as the various engineering-level steps required to translate and prepare a quantum circuit for execution on a quantum processor [11]. Central to the quantum compilation is the *quantum circuit-mapping problem* (QCMP), which concerns the assignment and rearrangement of qubits from an algorithm to a processor as a quantum circuit is executed, in order to guarantee high fidelity of the resulting state [12, 13]. It is known that the quantum

circuit-mapping problem is NP-complete [14, 15], and has been likened to the traveling salesman problem (TSP) on a torus [16]. The QCMP is also related to token swapping [17]. Many competing approaches have been proposed for solving the QCMP, with all of the state-of-the-art strategies trading accuracy for speed, among other considerations [18–34]. However, to our knowledge, no work has attempted to formulate the QCMP from a standpoint grounded in theoretical physics, specifically in quantum information theory. The motivation for such an endeavor is twofold. Firstly, since the QCMP is a physical process, such a description can provide new insights and perspectives on how best to solve it. Secondly, by providing a fundamental description of the QCMP, we lay the groundwork for uniting the various contemporary approaches towards a solution, and show how they relate to each other in a self-consistent framework. In short, a physics-motivated description of the QCMP offers consensus for current and future solution strategies, and how best to compare them.

Underpinning the advances in quantum technology, *quantum information theory* seeks to quantify the achievable limits of information processing on a fundamental mathematical basis using quantum physics [1, 35, 36]. While such progress is already notable, many fields outside of the immediate scope of quantum information theory have benefited from incorporating quantum-information-theoretic interpretations to outstanding research problems, including theoretical physics [37, 38], network science (which studies the behavior of complex networks from the standpoint of statistical mechanics and graph theory) [39–41], among many others. Bearing in mind such potential, we apply notions of quantum information theory, in particular, *quantum resource theory* [42, 43], *spectral graph entropy* [39, 44–46], and the *quantum opera-*

---

\* These authors contributed equally to this work.

tions formalism [35, 47–49] to the QCMP, in order to describe the problem of preparing certain quantum states on a quantum processor whose qubit connectivity is restricted. As a quantum circuit itself describes a sequence of unitary transformations under which a quantum state transforms, addressing such quantum operations under the guise of a processor’s connectivity is not only reasonable using quantum information theory, but also embodies a natural extension of quantum information theory to the setting of practical quantum computing.

Several recent proposals have sought to establish links between graph theory and the QCMP [28, 29, 50–52]. Since then, it has become commonplace in the literature to consider an *interaction graph* (IG), in which edges represent the necessary two-qubit interactions for implementing a quantum circuit, and a *coupling graph* (CG), whose edges determine allowed two-qubit interactions between neighboring subsystems on the processor [53]. In many of these proposals, the SWAP gate count required to realize a quantum algorithm on a given quantum processor is considered to be a typical metric for the objective function of a mapping strategy [22].

In this vein, we strengthen this connection by initiating a study of the QCMP from the standpoint of the quantum operations formalism, using notions from graph theory and network science as a foundation. More concretely, we propose a special case of the QCMP in which all two-qubit interactions of a given IG can be compressed into a single time slice of the quantum circuit. Starting from this point, we reformulate the QCMP as a *superoperator mapping* in the space of density matrices; as such, we employ *doubly-stochastic quantum operations* [49, 54], wherein both the initial density matrix represents the graph Laplacian of the associated IG, subject to the constraints of the CG. Using recent results in *resource theory*, *quantum circuit complexity* [42, 43], and methods from *quantum information geometry* [55], we methodically show that entropic divergence measures can be used in order to minimize the distance between density matrices describing the IG and CG, and that a minimal SWAP gate count can be ascertained for any IG / CG pair using this method. This minimal SWAP gate count is shown to exactly coincide with the *quantum circuit uncomplexity* [42, 43]; as such, we name this lower bound the *SWAP uncomplexity*.

In addition, we develop a novel algorithm for the *qubit assignment* (or initial placement) of qubits from the IG to the CG, based on a subgraph isomorphism and graph similarity search [56–58], which has applications for *multi-programming* on a quantum device [59] and may be of independent interest. In this case, however, it serves as a necessary step in our formulation and further enables our approach by constraining the coupling graph to match the size of an IG, which is one of the method’s crucial requirements. This algorithm also facilitates a calculation that we use to compute a maximal SWAP gate count.

Together with the formalism introduced, a combined approach is constructed that searches for the best qubit assignment in terms of the *graph-edit distance* (GED), and then calculates the SWAP uncomplexity, given an IG/CG pair as inputs. We test the resultant algorithm against IBM’s Qiskit

compiler, finding that in all cases, the SWAP gate count as calculated by the SWAP uncomplexity algorithm is never surpassed, serving as a useful proof of concept. This minimal bound is of great importance, as such resource constraints can help with the prediction of compilation performance, as well as for making design choices relevant in application-specific mapping strategies and quantum devices [8].

This article is organized as follows. We review the QCMP in Section II. Following this section, we immediately discuss in Section III how to mathematically map objects such as the *graph Laplacian* from graph theory into the density matrix formalism, highlighting in the process the importance of *entropic divergence measures* (Section III A). Next, we show in Section IV how to translate the QCMP in density-matrix form to a statement about quantum circuit complexity, and we describe how to optimize for a quantity known as *uncomplexity* [42, 43]. In Section V we describe an algorithmic implementation for calculating the SWAP uncomplexity; here we also treat several subtleties of the problem (Sections V A and V B). We present the numerical results from over 600 benchmarks tested on realistic quantum circuits and hardware layouts in Section VI. Next, a physical interpretation of the SWAP uncomplexity is given, using a Penrose diagram as a guide, in Section VII. Finally, we offer final conclusions and ideas for future work in Section VIII.

## II. QUANTUM CIRCUIT MAPPING

Generally, quantum algorithms and their associated circuit-level descriptions are developed without considering the architecture-specific limitations of particular devices, i.e., they are developed in an *architecture-free* manner. For example, the *elementary gate set* (or primitives) for a particular device may differ significantly from what has been indicated at the level of a generic circuit description; as such, several actions must be performed in order to translate the quantum algorithm into a circuit that a quantum device can actually execute. Another example can be seen in the physical connectivity properties of a quantum processor, which must be considered to ensure that the necessary qubit-qubit interactions of the circuit can be performed on the device. Although certain exceptions may exist (in which several of the aforementioned steps may not necessarily be carried out), these procedures are collectively known as *quantum circuit mapping* [11].

The task of quantum circuit mapping itself is usually divided into several steps which typify the process: A) *elementary gate-set decomposition*, which involves the translation of a circuit to a native gate set utilized by a quantum processor; B) *scheduling*, which concerns the formation of a logical time ordering for algorithm execution, and includes considerations for parallelism of operations and for the shortening of circuit depth; C) *qubit assignment*, which relates to the initial assignment of qubits from an algorithm to the physical qubits on a quantum architecture; and D) *qubit routing*, which examines the increase in gate overhead as extra operations are inserted into the algorithm as a function of physically moving qubits around the processor, such that the required two-qubit opera-

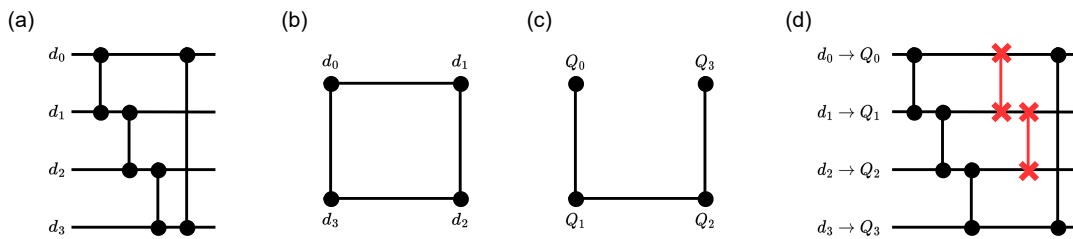


FIG. 1. An example of the QCMP as a sequence of steps needed to assign qubits from an algorithm to a quantum device. The two-qubit gates in the two circuit diagrams are used to represent general two-qubit unitary operations (with the exception of SWAP gates); here, we do not consider single-qubit gates, and the two-qubit interactions shown in (a) and (d) are taken to be general two-qubit unitary operations. (a) The quantum circuit is transformed into an *interaction graph*, as shown in (b). Next, it is compared with the connectivity properties of the *coupling graph* (c). As no *graph isomorphism* (i.e., no exact matching between the vertices of the IG and CG which upholds all of the edge relations of both) exists between the IG and CG, one can compensate for the lack of connectivity by introducing SWAP operations to the circuit in order to realize the circuit. (d) These operations degrade the fidelity of the final output state.

tions are realizable [11]. Typically, operations such as SWAP gates are utilized in order to adapt the circuit to hardware; these amount to classical permutation operations on a product state, but other approaches exist as well [32, 60, 61].

As a simple example, consider the quantum circuit-mapping procedure in Figure 1. The circuit on the left is decomposed into IG form (a)-(b), wherein we do not consider single-qubit gates for simplicity, and we assume that the two-qubit gates shown in the circuit diagrams are taken as general two-qubit operations. Upon comparing the IG with the available qubit-qubit interactions afforded by a quantum device, it is apparent that the connectivity available on the device and the connectivity required by the algorithm differ (the two-qubit interaction represented by the edge  $e_{d_0 d_1}$  is not possible, as shown in (b)-(c)). As such, this discrepancy can be compensated for by adding detrimental SWAP operations to the circuit's initial assignment (d). This example provides an illustration of *quantum circuit mapping* based on an exact graph matching between IG and CG. Implicit to this example was the assumption that exactly such a mapping between the vertices of the IG and CG exists which preserves all of the edge relationships of the IG; this is known as a *graph isomorphism*, and will be discussed in more detail in Appendix A.

In this paper, we formulate and solve a special case of the QCMP. In contrast to Figure 1, our formalism exhibits three main simplifications. Firstly, as is typical in the QCMP, we do not consider single-gate interactions in the formalism that we present starting in Section III. Secondly, we assume the existence of a noiseless quantum device, as such an ideal scenario precisely allows for the emergence of a lower bound. Finally, in real quantum hardware, typically we only consider that one multiqubit gate can be performed on a given hardware qubit during a given moment; this necessitates the division of the quantum circuit into time slices. Instead, we consider the scenario in which all two-qubit gate interactions of the circuit can be performed within a single unit time slice, i.e. the causal structure of our circuits are taken to be indefinite [62, 63]. We devote more detail to these concepts in Section VII.

### III. GRAPHS AS DENSITY MATRICES

In quantum physics, the most general manner of describing a quantum state involves the use of *density matrices* [1, 64]. A density matrix  $\rho$  is a Hermitian, positive semidefinite matrix, whose trace is equal to unity. A system  $|\psi\rangle$  is termed *pure* if and only if the bound  $\text{Tr}[\rho^2] \leq 1$  is saturated. The density matrix admits a spectral decomposition as

$$\rho = \sum_j p_j |\psi_j\rangle \langle \psi_j|, \quad (1)$$

for an orthonormal basis  $\{|\psi_j\rangle\}$ , where  $p_j$  are non-negative eigenvalues summing to 1.

The density matrix formalism allows one to define the *Von Neumann entropy* (VNE), which takes the form

$$\mathcal{S}(\rho) = -\text{Tr}[\rho \log \rho]. \quad (2)$$

Here we take the convention  $0 \log_2 0 := 0$ .

In this work, as in [39, 40], we make use of the concept of a density matrix to describe a complex network (i.e. a graph with many edges and vertices, and assumed topological structure [65]), by defining a matrix from a network which fulfills the mathematical properties of a density matrix. One such candidate was previously shown in [39] to be promising for adhering to the property of *subadditivity* for the VNE; this *Gibbs state* formulation is defined as

$$\rho_L = \frac{e^{-\beta \mathbf{L}}}{Z}, \quad (3)$$

where  $\rho_L$ ,  $e^{(\cdot)}$ ,  $\beta$ , and  $Z$  represent: the density matrix of graph Laplacian  $\mathbf{L}$ ; the matrix exponential; the inverse temperature (or diffusion time [44]); and the partition function, which is defined as  $Z = \text{Tr}[e^{-\beta \mathbf{L}}]$ , respectively. We define the graph Laplacian as  $\mathbf{L} := \mathbf{D} - \mathbf{A}$ , following [39, 66]. Throughout the text, we will refer to the graph Laplacians

for the IG and CG using the notation  $\mathbf{L}_{IG}, \mathbf{L}_{CG}$ , respectively, and  $\rho_{IG}, \sigma_{CG}$  to refer to their derived IG and CG density-matrix forms, respectively. Additionally, we refer to edges in a graph-theoretic context as a line connecting two vertices; in the density-matrix formalism, we will make reference to this instead with the term *subsystem interactions*.

Using these objects to describe complex networks is advantageous for several reasons. Firstly, although it is known that the graph Laplacian is uniquely determined up to vertex-numbering assignments [67], the *eigenvalue spectrum* of the graph Laplacian does not allow for unique identification of a graph. For example, two graphs can be *cospectral*, i.e. possessing the same eigenvalue spectrum, but with different connectivity [67]. As such, the approach we detail in this work is motivated by the fact that *entropic divergence measures* allow for a unique differentiation between two quantum states  $\rho$  and  $\sigma$ . Secondly, the VNE is *permutation-invariant*, i.e., the VNE is invariant under a reordering of subsystems. For example, suppose we have a state vector of five subsystems a, b, c, d, and e. If two such subsystem orderings give rise to density matrices  $\eta = \sum_{abcde \in \mathbb{Z}_2} |abcde\rangle \langle abcde|$  and  $\xi = \sum_{abcde \in \mathbb{Z}_2} |baced\rangle \langle baced|$ , it can be shown that the equality  $\mathcal{S}(\eta) = \mathcal{S}(\xi)$  holds [49]. Lastly, as discussed in [39, 40], previous attempts to calculate the classical entropy of a complex network fail, as these measures are dependent on a probability distribution resultant from a specific network descriptor. In contrast, the quantum approach we utilize does not depend on a specific network descriptor, but rather the entire network, rescaled and normalized as a Gibbs state.

### A. Entropic Divergence Measures

The task of actually distinguishing two quantum states  $\rho$  and  $\sigma$  can be accomplished through the use of the *entropic divergence measures* [1, 36, 45, 46, 49, 68, 69]. In particular, we employ the *quantum Jensen-Shannon divergence* (qJSD), which is defined as

$$\mathcal{D}_{qJSD}(\rho||\sigma) = \mathcal{S}\left(\frac{\rho + \sigma}{2}\right) - \frac{1}{2}(\mathcal{S}(\rho) + \mathcal{S}(\sigma)). \quad (4)$$

One may immediately ask why we choose to utilize the qJSD, and not other quantum entropic measures, such as the *mutual information* or the *quantum relative entropy* (QRE) [1]. The reason for this choice is severalfold, and is intimately related to the QCMP. Firstly, the qJSD defines a bounded *metric space* (see Appendix B). More specifically, we note that

$$0 \leq \sqrt{\mathcal{D}_{qJSD}(\rho||\sigma)} \leq 1, \quad (5)$$

with a value of 0 signifying that  $\rho = \sigma$ , and a value of 1 used for the case of  $\rho \perp \sigma$  [68, 70]. As we are comparing the density matrices related to the IG and CG of a quantum circuit and processor, it is imperative to understand the closeness of one to the other, using some bounded distance measure. As a contrasting incentive, consider measuring the QRE of two

orthogonal states; in this case, the divergence is unbounded and gives  $\mathcal{D}_{QRE}(\rho||\sigma) \mapsto \infty$  [1]. In the practical setting of the QCMP, such a measure is therefore not useful and does not convey the necessary distance information.

Secondly, the qJSD is *symmetric*. This property is concomitant to the previous property related to metric spaces, but we address it here separately. Symmetricity means that the qJSD obeys the relation

$$\mathcal{D}_{qJSD}(\rho||\sigma) = \mathcal{D}_{qJSD}(\sigma||\rho). \quad (6)$$

For the QCMP, we observe that this relation is desirable, as we wish for the notion of distance between two density matrices to stay the same, regardless of whether one is derived from  $\mathbf{L}_{IG}$  or  $\mathbf{L}_{CG}$ . As we will see in Section IV, it is in fact this distance quantity that we relate to the *quantum circuit uncomplexity* [42, 43]. Additionally, the concept of symmetricity is paramount, as it permits us to directly relate the qJSD to the *Fisher information metric*; it was in fact shown through application of the Fubini-Study metric that the qJSD is directly related to the *thermodynamic distance* between two equilibrium quantum states, and lower bounds their divergence on a Riemannian manifold [71].

Moreover, the qJSD is *non-increasing* under the action of a CP map [68], which can be formally stated as

$$\mathcal{D}_{qJSD}(\rho||\sigma) \leq \mathcal{D}_{qJSD}(\Lambda(\rho)||\Lambda(\sigma)), \quad (7)$$

where  $\Lambda(\cdot)$  represents the superoperator of a *quantum operation*. The most general form of a quantum operation can be written in several representations; in this work we will concentrate on the Kraus representation (also known as the *operator-sum* representation), stated as

$$\Lambda(\cdot) := \sum_i E_i \cdot E_i^\dagger, \quad (8)$$

where  $E_i$  is the  $i^{\text{th}}$  term in the sum of operators, and  $\Lambda(\cdot)$  is taken to be a general quantum operation superoperator, constrained to the *completely-positive* (CP) condition [1, 35, 36].

We also introduce here the class of *doubly-stochastic* (DS) quantum channels, with the term *quantum channel* distinguishing from *quantum operation* in that, in addition to the CP constraint, we additionally impose *trace preservation* (TP) [1]. In this work, we will refer to CPTP maps using  $\Phi(\cdot)$ . Moreover, DS quantum channels are *unital*, meaning that the fixed point of the channel upholds the equality  $\Phi(\mathbb{I}_n) = \mathbb{I}_n$  [47, 49]. In defining the class of DS quantum channels, we use the fact that any Kraus operator can be factorized, as all systems of Kraus operators implementing a quantum operation are related by a unitary transformation. A particular decomposition can be defined as

$$E_i = \sum_j \sqrt{\theta_j} P_j. \quad (9)$$



Here  $P_j \in \mathbb{P}_n$  refers to permutation matrices from the set of  $n \times n$  permutation matrices, and  $\theta_j$  refers to a probability distribution [49]. The existence of this class of convex decomposition comes from the *Birkhoff-Von-Neumann Theorem* [36, 49, 54] for which it is known that such a decomposition can be found in polynomial time [72].

Lastly, we introduce the notion of *projective measurements* for density matrices constructed from graph Laplacians. Following the treatment of [41], we define a set of orthogonal projectors  $\Pi_k$  such that  $\sum_k \Pi_k = \mathbb{I}_n$ . The post-measurement state of a general density matrix  $\rho$  is  $\frac{\Pi_i \rho \Pi_i}{\text{Tr}[\Pi_i \rho]}$ , where  $\text{Tr}[\Pi_i \rho]$  represents the probability of the  $i^{\text{th}}$  measurement outcome. Note that projective measurements are known as a specific example of a CP map [1, 35, 36]. In Section IV, we shall use projective measurements to erase subsystem interactions from the density-matrix form of the IG,  $\rho_{\text{IG}}$ , as well as for selecting appropriate subsystem permutations of the CG density matrix  $\sigma_{\text{CG}}$ .

#### IV. QUANTUM CIRCUIT MAPPING AS A RESOURCE THEORY

In the QCMP, if graph Laplacians  $L_{\text{IG}}$  and  $L_{\text{CG}}$  exactly match, i.e. if  $L_{\text{IG}} = L_{\text{CG}}$ , then all of the necessary two-qubit interactions from the IG can be performed on the CG without further circuit modification, effectively requiring zero SWAP gate insertions. Similarly, as discussed in Section III A, if  $\mathcal{D}_{\text{qJS}}(\rho_{\text{IG}} \parallel \sigma_{\text{CG}}) = 0$ , then we can analogously conclude that  $\rho_{\text{IG}} = \sigma_{\text{CG}}$ , and all subsystem interactions from the IG are realizable on the CG without the addition of SWAP gates. We will consider this case to be trivial from the standpoint of the QCMP.

Under these conditions, the qJSD provides an efficient method to check whether a quantum circuit is implementable on a given quantum device. However, one might wonder how to address the case of  $\mathcal{D}_{\text{qJS}}(\rho_{\text{IG}} \parallel \sigma_{\text{CG}}) \neq 0$ , which is the aim of this work; in order to confront this, we return to physical considerations of the problem.

We first address how to ascertain exactly which two-qubit interactions are not possible on the quantum device. This aim can be accomplished by means of projective measurements; the idea here is to simply project out all two-qubit interactions from  $\rho_{\text{IG}}$  which are already possible on  $\sigma_{\text{CG}}$ . From [41] it was shown that the graph operation known as *edge removal* was possible by considering projective measurements, which are known to be CP operations. As such, our overarching goal will be to *erase all of the subsystem interactions* from  $\rho_{\text{IG}}$  as quickly as possible, as this corresponds to all of the circuit two-qubit gates being accounted for on the device. Firstly, we define a new density matrix  $\rho_{\text{IG}}^i$  as

$$\rho_{\text{IG}}^i := \Pi_{\bar{E}} \rho_{\text{IG}} \Pi_{\bar{E}}, \quad (10)$$

where the projectors  $\Pi_{\bar{E}}$  leave only those subsystem interactions which are in the IG's edge set  $E_{\text{IG}}$  but not in the CG's edge set  $E_{\text{CG}}$ , i.e.  $\bar{E} = E_{\text{IG}} \setminus E_{\text{CG}}$ . The superscript  $i$  refers

to the  $i^{\text{th}}$  iteration of edge removal performed on the original  $\rho_{\text{IG}}$ .

Once  $\rho_{\text{IG}}^i$  is derived from its modified graph Laplacian, the erasure process can commence. In order to erase a subsystem interaction from  $\rho_{\text{IG}}^i$ , we must first permute a pair of subsystems from  $\sigma_{\text{CG}}$  such that the corresponding interaction becomes possible on the device.

Let us imagine first, as a simple scenario, that  $\rho_{\text{IG}}^i$  contains only one subsystem interaction remaining. In order to permute the subsystems of  $\sigma_{\text{CG}}$ , we employ the DS quantum channels introduced in the previous section. The resulting calculation proceeds as

$$\mathcal{D}_{\text{qJS}}(\rho_{\text{IG}}^i \parallel \Phi(\sigma_{\text{CG}})) \geq 0, \quad (11)$$

where  $\Phi(\sigma_{\text{CG}}) = \sum_j \theta_j P_j \sigma_{\text{CG}} P_j$ . There is one subtlety to this point. Not every possible permutation matrix in  $\mathbb{P}_n$  can be defined for the DS quantum channel, as we are limited by the connectivity of the quantum device. In view of this, we restrict  $P_j \in \mathbb{P}_n^{\text{CG}}$ , where  $\mathbb{P}_n^{\text{CG}}$  represents the permutation matrices allowed by the available two-qubit interactions in  $E_{\text{CG}}$ .

As the superoperator  $\Phi(\sigma_{\text{CG}})$  yields a superposition of possible permutation choices, one may ask then how to decide on which permutation to apply to  $\sigma_{\text{CG}}$ . In order to resolve this complication, we perform a projective measurement corresponding to the permutation matrix appearing in the Kraus operator which obtains the largest value of  $\theta_j$ . Conversely, if we obtain several values of  $\theta_j$  which are equal (this can happen in larger complex networks, where several shortest paths of permuting subsystems exist), we make no distinction as to which component is chosen (in Section V, we treat this issue in the practical sense by employing an optimization algorithm based on gradient descent from the Python package SciPy [73]). The physical motivation for this procedure can be justified from tools in *quantum information geometry* [55].

It is well known in quantum information geometry that the distance between two equilibrium quantum states can be parameterized by the *Fubini-Study metric* [42, 55, 74]. This metric in turn can be shown to be a special case of the *Fisher information metric* applied to projective Hilbert spaces. The Fisher information metric is also directly related to the qJSD [71]. In light of this knowledge, minimizing the qJSD is then immediately associated with a minimization of the *thermodynamic path length* between two equilibrium quantum states, and thus lower bounds their distance on a Riemannian state space manifold. Additionally, it is known that VNE monotonically increases under the action of a CP map [75]. Therefore, we argue that by performing a selection of the maximum-probability permutation matrix on  $\sigma_{\text{CG}}$ , we in effect choose the quantum operation which minimally increases the VNE, ergo minimizing the qJSD between  $\sigma_{\text{CG}}$  and  $\rho_{\text{IG}}^i$ .

As such, we modify Equation 11 in order to accommodate this choice as a projective measurement:

$$\min_{\theta} \left[ \mathcal{D}_{\text{qJS}}(\rho_{\text{IG}}^i \parallel \Pi_{\theta_{\text{max}}}(\Phi(\sigma_{\text{CG}}))) \right] \geq 0. \quad (12)$$

Here,  $\Pi_{\theta_{\max}}$  signifies a projective superoperator map onto the maximum-probability  $\theta_{\max}$  after minimizing. If we require several subsystem permutations before reaching the minimal value of qJSD, then we simply extend the map by defining a composition of such quantum operations as  $\xi(\cdot) = \Pi_{\theta_{\max}}(\Phi(\cdot))$ , and the action of these operations can be written concisely as  $\xi^{\circ l_i}(\cdot) = \Pi_{\theta_{\max}}^{l_i}(\Phi^{l_i}(\dots \Pi_{\theta_{\max}}^1(\Phi^1(\cdot))))$ , where the superscript  $l_i$  refers to the  $l_i^{\text{th}}$  superoperator composition for the  $i^{\text{th}}$  remaining subsystem interaction in  $\rho_{\text{IG}}^i$ . This can be amended to Equation 12 as

$$\min_{l_i} \left[ \min_{\theta} \left[ \mathcal{D}_{\text{qJS}}(\rho_{\text{IG}}^i || \xi^{\circ l_i}(\sigma_{\text{CG}})) \right] \right] \geq 0. \quad (13)$$

Equation 13 still only takes into account *one* possible subsystem interaction remaining on  $\rho_{\text{IG}}^i$ , however. We may generalize this logic further for  $|E_{\text{IG}}|$  subsystem interactions remaining in  $\rho_{\text{IG}}^i$ , such that many possible remaining subsystem interactions can be treated:

$$\Pi_i \left[ \min_{l_i} \left[ \min_{\theta} \left[ \mathcal{D}_{\text{qJS}}(\rho_{\text{IG}}^i || \xi^{\circ l_i}(\sigma_{\text{CG}})) \right] \right] \right]_{i \in \bar{E}_{\text{IG}}} \geq 0. \quad (14)$$

Here,  $\Pi_i[\cdot]$  represents the projective superoperator map which erases the  $i^{\text{th}}$  subsystem interaction from  $\rho_{\text{IG}}^i$ . In the end, we successfully project out all of the subsystem interactions from  $\rho_{\text{IG}}^i$ , as they become realizable on the quantum device denoted as  $\sigma_{\text{CG}}$ . After the final step,  $\rho_{\text{IG}}^i = \mathbb{I}_n$ .

However, we can further sum all of the gate operations which were required in order to transport  $\sigma_{\text{CG}}$  as close as possible to all of the  $\rho_{\text{IG}}^i$ . Indeed, summing over the collected  $l_i$  permutations per subsystem interaction  $i$  allows us to find the minimal SWAP gate count for performing a circuit on a device. Continuing, we are left with the equation

$$\sum_i^{\bar{E}} l_i = \mathcal{C}(\mathbb{I}_n) - \mathcal{C}(\sigma_{\text{CG}}) = U_{\text{SWAP}}, \quad (15)$$

where  $U_{\text{SWAP}}$  represents the *SWAP uncomplexity* between  $\rho_{\text{IG}}^{i_{\max}} = \mathbb{I}_n$  and  $\sigma_{\text{CG}}$  [42, 43], and  $\mathcal{C}(\cdot)$  signifies the *quantum circuit complexity*. It is known that quantum circuit uncomplexity defines a *resource theory* and can be optimized for [76]. As it is known that most states of maximal circuit complexity are maximally mixed [42], the formalism presented here portrays a precise lower bound distance measure in terms of SWAP gates required for executing a quantum circuit on a quantum device.

## V. ALGORITHMIC IMPLEMENTATION

Pseudocode for calculating the SWAP uncomplexity is shown in Algorithm 1. The algorithm proceeds in a very similar form to the mathematical breakdown. Firstly, the density-matrix objects  $\rho_{\text{IG}}$  and  $\sigma_{\text{CG}}$  are initialized and provided as

input for the algorithm;  $U_{\text{SWAP}}$  is set to zero. Next, the algorithm described in Section VB is used to determine the optimal initial assignment of qubits from  $\rho_{\text{IG}}$  to the qubits of  $\sigma_{\text{CG}}$ . The object  $\rho_{\text{IG}}^{i=0}$  is generated using the projective measurement approach detailed in Section IV. Once an initial assignment is completed, an orientation of the two density matrices to each other is set, and they can be compared using the qJSD. If the value of the qJSD is initially zero, then both of the density matrices are the same, and no SWAP gates are necessary. However, if the qJSD is non-zero, we then perform a minimization of the divergence, allowing for permutations of subsystems in  $\sigma_{\text{CG}}$  via the DS quantum channel; the minimization takes place over the vector of squared probabilities  $\bar{\theta}$ . As a result of the optimization, the permutation matrix whose associated  $\theta_j$  value is highest is selected and performed on the device, in agreement with previous observations on the minimization of thermodynamic length via the Fisher information metric [71, 77]. The superscript  $l$  is used to count the number of iterations of the DS quantum channel as the algorithm proceeds. Continuing, the divergence of the newly-modified CG density matrix,  $\xi^{l+1}(\sigma_{\text{CG}})$ , should be *lower* than before. If instead it is found that the divergence is not lower (or is the same), then the previous iteration,  $\xi^l(\sigma_{\text{CG}})$ , is taken to the next step of the algorithm. The optimization scaling for this calculation is expected to be  $\mathcal{O}(n^2 + c)$ , as is dictated by the convexity of the problem [72]. Finally, we check explicitly to see if  $\rho_{\text{IG}}^i = \mathbb{I}_n$ ; if it is, then we first sum the  $l_i$  in the variable  $U_{\text{SWAP}}$  and immediately stop the algorithm, as our goal of erasing subsystem interactions in  $\rho_{\text{IG}}$  is achieved. If not, we proceed to remove additional subsystem interactions from  $\rho_{\text{IG}}^i$ , generating a further iterated object  $\rho_{\text{IG}}^{i+1}$ .

At this point, the erasure of a remaining subsystem interaction implies that the qJSD will again increase, as we know that the VNE under a CP map always increases [75]. We must then perform the commensurate DS quantum channel operation(s) again and select the appropriate  $\theta_j$ -valued permutation such that the divergence decreases to its minimal value once more. The algorithm terminates upon the successful erasure of all subsystem interactions in  $\rho_{\text{IG}}^i$ , leaving a maximally mixed state. Once this is completed, we sum all of the collected  $l_i$  for each edge  $i$ ; this sum is then taken as the SWAP uncomplexity  $U_{\text{SWAP}}$  and is returned.

### A. The $\beta$ Parameter

One of the subtleties of our algorithmic implementation lies in the estimation of an appropriate value for the inverse temperature  $\beta$ , and can be tricky. As shown in Figure 2, we have graphed the value of  $\beta$  versus the VNE in the resulting density matrix. The figure depicts a dependency of the VNE on  $\beta$ . As shown, a phase transition is present at and about the point of  $\beta \sim 10^0$ , while the *high-temperature regime* generally begins at  $\beta \sim 10^{-1}$  and extends leftwards. In this work, we search over a range of  $\beta$  values with varying increments; the preferred value yields the minimal SWAP gate count for an IG and CG pair. We were able to ascertain this minimal SWAP gate count using a search over the range of  $10^{-5} \leq \beta \leq 10^5$ .

---

**Algorithm 1:** Pseudocode for SWAP Uncomplexity  $U_{\text{SWAP}}$ .

---

**Input:**  $\rho_{IG}, \sigma_{CG}$   
Initial\_Qubit\_Assignment  $\leftarrow$  Qubit\_Assignment( $\rho_{IG}, \sigma_{CG}$ )  
 $U_{\text{SWAP}} \leftarrow 0$   
**Output:**  $U_{\text{SWAP}}$   
**Assert:**  $\mathcal{D}_{qIS}(\rho_{IG} || \sigma_{CG}) == 0$

```

if  $\mathcal{D}_{qIS}(\rho_{IG} || \sigma_{CG}) \neq 0$  then
   $\rho_{CG}^{i=0} \leftarrow$  Remove_Trivial_Edges( $\rho_{CG}$ )
  for  $i \in [0, |E_{IG}|]$  do
    for  $l_i \in [0, |E_{CG}|]$  do
       $qj\text{sd}_1 \leftarrow \min_{\bar{\theta}} \left[ \mathcal{D}_{qIS}(\rho_{IG}^i || \sum_j \theta_j P_j \sigma_{CG} P_j) \right]$ 
       $\xi^{l_i+1}(\sigma_{CG}) \leftarrow \Pi^{\max} [\theta_j P_j \sigma_{CG} P_j] \Pi^{\max}$ 
       $qj\text{sd}_2 \leftarrow \min_{\bar{\theta}} \left[ \mathcal{D}_{qIS}(\rho_{IG}^i || \xi^{l_i+1}(\sigma_{CG})) \right]$ 
      if  $qj\text{sd}_2 < qj\text{sd}_1$  then
        continue
      else
         $U_{\text{SWAP}} \leftarrow U_{\text{SWAP}} + l_i$ 
        break
      end if
    end for
  end for
  if  $\rho_{IG}^i == \mathbb{I}_n$  then
     $U_{\text{SWAP}} \leftarrow U_{\text{SWAP}} + l_i$ 
    break
  else
     $\rho_{IG}^{i+1} \leftarrow$  Remove_Trivial_Edges( $\rho_{IG}^i$ )
  end if
end for
end if
return  $U_{\text{SWAP}}$ 

```

---

Keeping this matter in mind, the definition of SWAP uncomplexity states that *there exists a minimal bound* for the number of SWAP gates at *some value* of  $\beta$ , but does not say directly how one may find the most appropriate  $\beta$ , consistent with  $U_{\text{SWAP}}$ . As we show in Section VI, it so happens that almost all of our results ( $\sim 97\%$ ) achieve the minimal SWAP-gate count in the *high-temperature regime*, largely following the empirically-derived results of [78]. We will discuss possible improvements to this technique in Sections VII and VIII.

### B. Qubit Assignment

As mentioned previously in Section II, the initial stage of the QCMP is known as *qubit assignment* (also known as initial placement, qubit allocation, or initial mapping) [51, 52]. This procedure plays a pivotal role in quantum circuit execution [12]. In our proposal for calculating the SWAP uncomplexity in the QCMP, we also must assign qubits from the IG to the CG initially in an optimal way, as this influences how many SWAP gates will be utilized.

In [51], the concept of qubit assignment was introduced as a search for a subgraph isomorphism for an IG/CG pair. To our knowledge, this technique has not yet seen widespread implementation in practical qubit-assignment techniques, de-

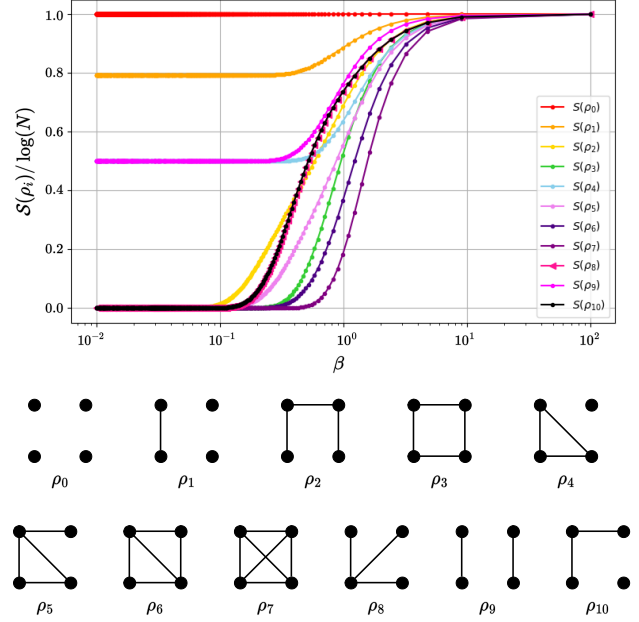


FIG. 2. The fluctuation of  $S_G(\rho_i)$  as a function of  $\beta$  for 4-node graphs. We have utilized different marker types in order to distinguish curves with very similar VNE.

spite its potential. Instead, most existing approaches focus on alternative factors such as sequential gate flow in the circuit or the number of interactions between qubits like in [20, 79, 80]. Nevertheless, some work has explored the subgraph-isomorphism concept for the QCMP [28, 52, 81, 82].

Building upon the foundation of the well-known VF2 algorithm [28, 83], our approach to qubit assignment searches for an exact location on the quantum device where our circuit can run without requiring additional gates. If a solution is feasible, we are left with an optimal assignment. In cases where a solution is not possible, we conduct a graph similarity search. This process involves the GED calculation and comparison of the IG to all distinct subgraphs of the same size within the CG, which opens up alternative assignment possibilities. In this fashion, we condense the search space for alternative solutions, while also highlighting the potential utility of our approach for *multi-programming* applications (i.e. executing multiple circuit in parallel on a quantum device) [59].

Let  $|V_{IG}|$  be the number of qubits in the IG, and  $|V_{CG}|$  be the number of physical qubits on the CG, as per the definitions from previous sections. Our qubit assignment process consists of the following steps:

#### 1. Preprocessing:

- (a) Select a quantum algorithm described as a quantum circuit and extract its interaction graph  $G_{IG}(E_{IG}, V_{IG})$ , where  $|E_{IG}|$  represents the number of edges in the IG.
- (b) Choose a quantum device to execute the circuit on and extract its CG, represented as graph  $G_{CG}(E_{CG}, V_{CG})$ , where  $|E_{CG}|$  stands for the number of edges in the CG.

- (c) In order to increase the efficiency of steps later on, and reduce the search space, we find all distinct subgraphs of size  $|V_{IG}|$  within graph  $G_{CG}$ .
2. *Subgraph isomorphism using VF2 and subgraph similarity search:*
    - (a) Use the VF2 algorithm to check if a subgraph isomorphism exists between graphs  $G_{IG}$  and  $G_{CG}$ .
      - i. If a subgraph isomorphism is found, we immediately determine the location within the CG for qubit assignment.
      - ii. When a subgraph isomorphism does not exist, we utilize the *graph-edit distance* (GED) (Appendix A) to identify structurally most similar subgraph of the CG when compared to the IG. During this process, we compare IGs only to distinct subgraphs of a CG derived from Item 1c.
    - (b) Assign the IG to the CG in accordance with the result from the previous step.
  3. *Calculating the maximal SWAP gate count* as it is qubit assignment-dependent. We describe the computation of this bound in more detail in Appendix C.

The steps in the algorithm are exemplified in Figure 3. Here, we take as a simple example the case of a 4-qubit IG assigned to a 7-qubit architecture, as shown in (a). In (b), we display the two distinct 4-qubit subgraphs that are identified in Item 1c. Finally, in (c) we show the final assignment of qubits as ordered pairs; in this case, an graph isomorphism was not found. Therefore, we select the subgraph with the lowest GED calculated, as per Item 2(a)ii. The final initial placement and related information obtained during this process serve as inputs for the SWAP uncomplexity algorithm, as described in Sections IV and V.

In addition to implementing the technique described above, a specific approach for *complete graphs* (i.e., all-to-all IGs) was utilized. For such cases, we automatically locate the most-connected subgraph of that size within the CG. This method can also be applied to circuits larger than 20 qubits. However, for the purpose of this paper, we focus on smaller circuits as a demonstration of the concept.

## VI. BENCHMARK EVALUATION & RESULTS

Here we describe numerical results taken from comparing the SWAP uncomplexity against IBM’s Qiskit compiler [84]\*, as well as against a brute-force approach [85]. These experiments were carried out for several reasons. Firstly, as the SWAP uncomplexity algorithm does in fact solve for the minimal SWAP gate count, then we should be able to confirm this fact by comparing with any compiler. By such logic, a compiler should be able to approach but not find fewer SWAP gates for an arbitrary IG / CG pair. In order to perform this empirical check, we choose to run our algorithm (Section V) against the Qiskit compiler. As the Qiskit compiler is considered to be the state-of-the-art approach at the moment, re-

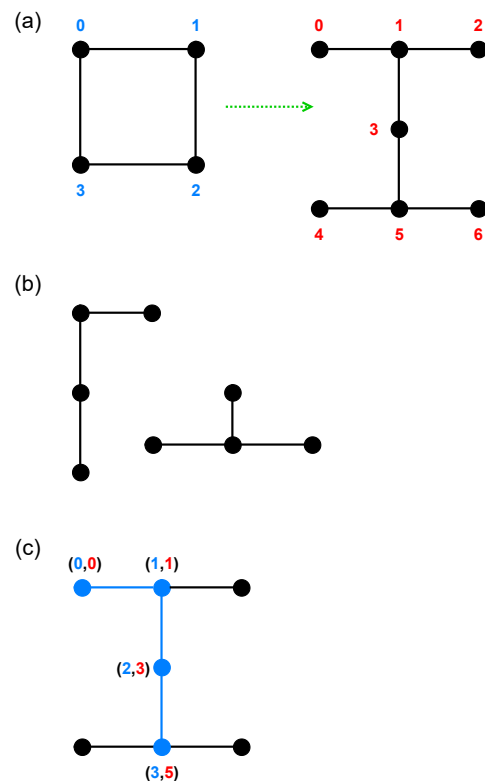


FIG. 3. Steps taken for the qubit-assignment algorithm described in Section VB: (a) The task at hand is to find the best-fit initial placement for the qubits in the 4-qubit IG (shown with blue numbering) for the 7-qubit CG (shown with red numbering); in our case, the CG corresponds to the connectivity of the *IBM Casablanca* quantum device. (b) Shows the distinct subgraphs found from Item 1c in Section VB. After verifying that no direct subgraph isomorphism between IG and one of these graphs exists, a similarity search is employed. (c) The subgraph of the CG with the lowest GED relative to an IG is retrieved. The resulting initial placement is shown in blue, with the final GED calculated to be 1. The actual qubit assignment is shown in the form of several colored ordered pairs (blue numbering represents IG qubits, while red numbering represents CG qubits).

alizing such a comparison provides a practical first test. Secondly, to the best of our knowledge, there is scant literature on bounding the required SWAP gates, and such work addresses only up to quantum circuits of 6 qubits via a brute-force optimization algorithm [85, 86]. Our simulation results demonstrate scalability that greatly exceeds the current state of the art [85], as we achieved results for circuits of up to 16 qubits.

57 benchmark circuits were selected from the *qbench* suite [53]. These benchmarks cover a range of 3 to 20 qubits and represent a wide spectrum of possible IG connectivities (47 different connectivities) encountered in quantum algorithms. More details about the selected benchmarks can be found in Table II. As for the CGs, we chose connectivity graphs from a set of 16 in-use quantum devices, ranging from 5 to 72 qubits.

\* Used version of Qiskit is 0.24.1.



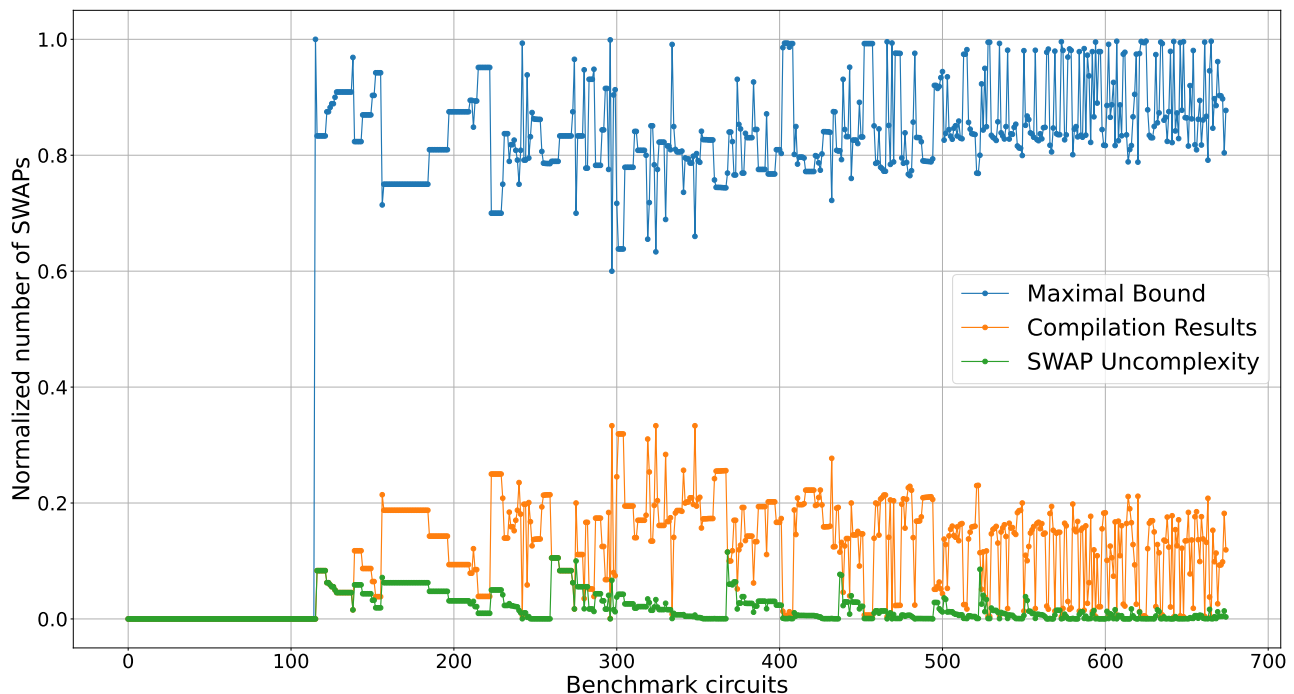


FIG. 4. Simulation results for various IG / CG benchmark pairs. The X-axis enumerates each benchmark circuit tested, and the Y-axis describes the normalized number of SWAPs, due to very high maximal bounds (the SWAP-bound values of each benchmark are divided by their sum). The results are color-coded as follows: the SWAP uncomplexity of Section IV (green); the Qiskit compiler with default options Sabre router and circuit optimization level 1 [84] (orange); and the maximal maximal bound calculated as in Appendix C (blue). In every IG/CG pair, the bound calculated captures the SWAP uncomplexity that is either approachable or unattainable by the Qiskit compiler, thus empirically demonstrating our formulation.

The specific details of these devices are provided in Table I. As some of the benchmarks are too large to be run on some of the smaller processors from our list, in total we devised 675 simulation experiments with the Qiskit compiler [84]. In these simulations, we utilized Qiskit’s transpiler with the default circuit-optimization setting.

The results of our simulations are shown in Figures 4–6. In Figure 4, we display the normalized number of SWAP gates found by: the SWAP uncomplexity from Section IV (shown in green); the Qiskit compiler (orange); and the maximum SWAP gate count (which we name  $\mathcal{M}_{\text{SWAP}}$  in Appendix C) (blue). We observe that the SWAP uncomplexity can be reached, but never surpassed by the Qiskit compiler for select benchmark trials. As expected, the Qiskit compiler significantly outperforms the maximum SWAP gate count calculated.

The non-triviality of the maximal and minimal SWAP gate counts becomes evident in Figure 5, where we present a matrix with correlation coefficients whose values range from  $-1$  to  $1$ , with  $0$  indicating no correlation [87]. This matrix compares the results that we obtained throughout the simulation; in particular, we compare the effective correlation between the SWAP uncomplexity; the Qiskit compiler SWAP calculation results; and the maximal bound as calculated in Appendix C. Notably, both of our bounds (i.e., those obtained from our minimal bound with the SWAP uncomplexity algorithm, as well as the maximum SWAP gate count) exhibit a substantial

positive correlation (34% and 73%, respectively) with the actual results obtained from the compiler. The correlations here exemplify the non-triviality of the bounds; in other words, the SWAP uncomplexity and maximal bounds grow proportionally with the actual compilation results. The results at best coincide with each other, meaning that the lower bound equals the actual SWAP gate count from the presence of a graph isomorphism; in this case, the SWAP uncomplexity, Qiskit result, and the maximal bound all obtain the same amount (which is zero if a graph isomorphism is present). These checks provide not only hard evidence for the usability of our methods, but additionally serve as pragmatic sanity test for our algorithmic implementations.

Although not shown in Figure 5, it is also worth observing the considerable impact of the initial placement on retrieving bounds, which particularly depends on the GED and the number of missing edges in the chosen CG partition compared to the IG. We therefore calculated the correlation coefficients of these two parameters as well when compared to our retrieved bounds, resulting in correlations of 79% and 61% for the SWAP uncomplexity and maximal bounds, respectively). Furthermore, using the same initial placement for the Qiskit compiler resulted in a 45% correlation with the initial placement-related parameters.

Additionally, our exact qubit assignment method was initially tested with 729 benchmarks, showing a success rate of 92.6%. The remaining 7.4% of the benchmarks could not

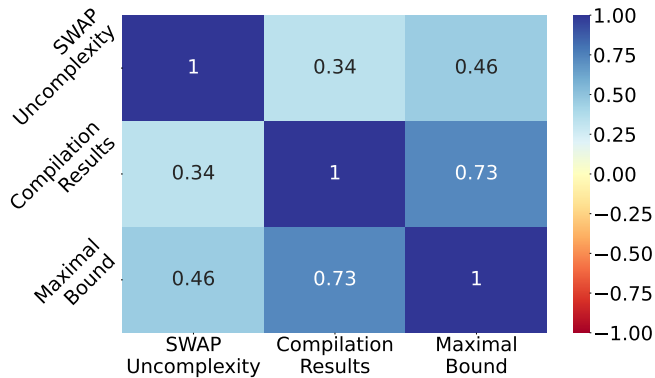


FIG. 5. The Pearson correlation matrix [87] between the critical parameters measured for our benchmark investigation. The values range between  $-1$  and  $1$  for negative and positive correlation, respectively. When one of the parameters changes, the other one changes in the same direction. In this figure, we observe a high positive correlation between all the selected parameters where the Pearson correlation coefficient ranges between  $0.34$  and  $1.0$ .

be finished due to insufficient computing resources (memory, long runtime, etc.). Recognizing the limited scalability of the approach (up to 16 circuit qubits), we developed a more relaxed method for complete graphs, mentioned in Section VB. Indeed, the scalability of our exact algorithm already exceeded that of the exact state-of-the-art algorithms, which struggled beyond 6 qubits [51]. Furthermore, our initial placement encountered no difficulties in exploring a vast search space. It successfully executed circuits on all tested devices, extending up to a size of 72 physical qubits in our case.

Figure 6 displays the  $\beta$  values obtained during the course of the simulation. As we must search over a range in order to find the most-appropriate  $\beta$ , it is helpful and interesting to catalog roughly how many benchmarks exhibited the minimal bound obtained and at which  $\beta$  values. In particular, we find that the vast majority of the benchmark pairs ( $\sim 97\%$ ) led to minimal SWAP counts within the range of  $\sim 10^{-5} - 10^{-3}$ , consistent with the *high-temperature regime* studied in [78]. We will comment on this more in Section VII.

Lastly, Figure 7 shows the results of a comparison leveraged between our SWAP uncomplexity algorithm (Section V) and the brute-force optimization results from [85]. In this approach, the authors utilize an optimizer which essentially tries every permutation of SWAP placements which is possible, respecting the gate-dependency graph and weighted IG of the original quantum circuit. In all cases, we see clearly that the brute-force algorithm only achieves the minimal bound, but never surpasses it.

## VII. DISCUSSION

It is known that the QCMP is NP-complete [14]. We have made three simplifications in order to derive the SWAP uncomplexity. Firstly, we do not consider single-qubit interac-

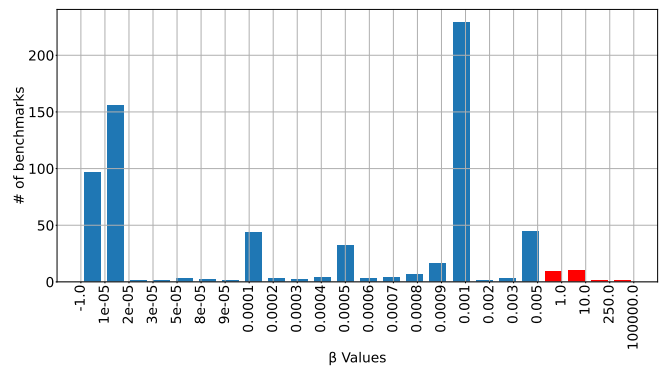


FIG. 6. The distribution of  $\beta$  values for minimal bounds found by the SWAP uncomplexity algorithm. Results in blue ( $\sim 97\%$ ) were found in the high-temperature regime described in [78]. We searched values in the range from  $10^{-5} - 10^5$  based on the following formula  $A * 10^a$  where  $A \in 1, 2, 3 \dots 9$  and  $a \in -5, -4, \dots, 4, 5$ .

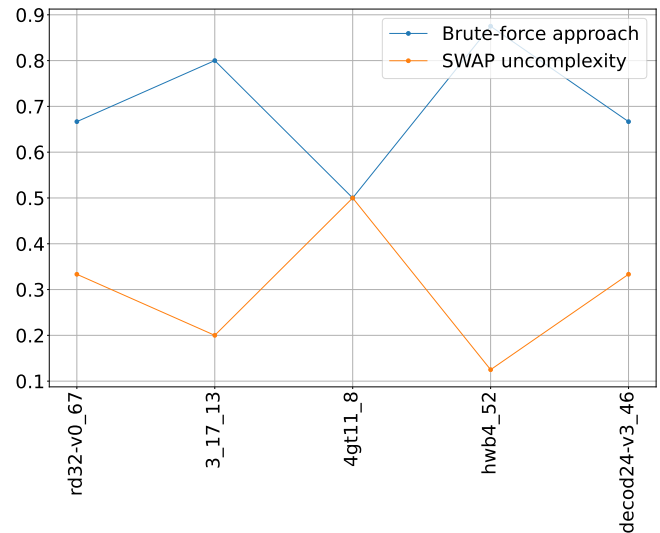


FIG. 7. Comparison of our minimal bounds with results of [85]. We notice that, just like before, our results (shown in orange) are always smaller or equal to the actual number of SWAPs. The benchmarks employed in this study are identical to those utilized in [85]. The results were normalized in the same way as in Fig. 4.

tions, as it is known that such gates do not heavily affect calculated success rates [13]. Secondly, we have removed all two-qubit interaction noise from the coupling graph; this should come as no surprise, as we are mainly interested in finding a lower bound for the number of SWAP gates required, and such a lower bound mandates the existence of a hypothetically noiseless quantum processor. Thirdly, we consider the limit in which gate dependencies for the IG are not considered; implicitly, we assume the existence of not only a noiseless quantum processor, but additionally one that can perform all two-qubit gate interactions required in one unit time slice.

At the outset, one may consider a graph-theoretic interpretation of the SWAP uncomplexity as considering only connectivity dissimilarities between the interaction and coupling

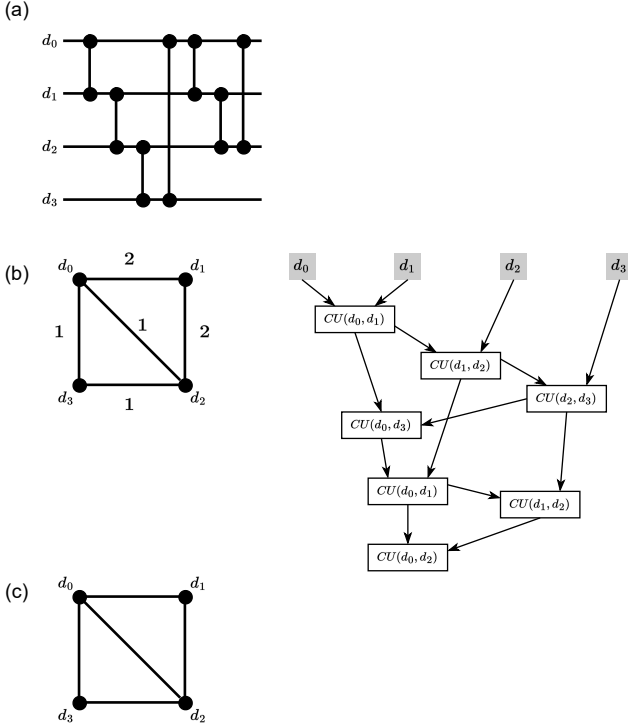


FIG. 8. Distinctions between the standard IG and the minimal version of the same IG. (a) illustrates an archetypal quantum circuit with arbitrary CU interactions, although making an exception with SWAP gates. (b) displays the standard weighted IG, together with its corresponding gate-dependency graph; we follow the gate-dependency notation used in [88]. (c) shows the unweighted form of our IG; here we do not take into account the gate ordering nor the number of gate calls realized per qubit, opting instead towards an unweighted IG.

graphs. Indeed, not only are gate dependencies explicitly not taken into account, but we assume that qubits can interact with each other potentially an infinite number of times within a unit time subdivision of a compiler’s scheduling scheme. These differences are shown in Figure 8. In (a), we depict a generic quantum circuit, again omitting the single-qubit gates and taking every two-qubit gate shown to be a general CU gate for simplicity (the obvious exception to this rule would be the use of SWAP gates). In (b) the standard weighted IG and its accompanying gate-dependency graph are shown, following the notation of [88]. Finally, (c) makes manifest the differences between the standard IG for the QCMP and for our unweighted version. Here, we take any number of two-qubit interactions to 1 on the IG, and we omit the gate-dependency graph, preferring an indefinite causal structure.

Such a graph-theoretic picture as ours can be related using *Penrose diagrams* [89, 90], as shown in Figure 9. A Penrose diagram typically shows the causal structure of events unfolding in a *spacetime geometry* [89]. In Figure 9, the horizontal axis refers to purely spatial evolutions, which in our case are shown by potential SWAP erasures. Each of the sets outlined in orange represent elements of the same total number of edges, but different spectral properties. Each graph within

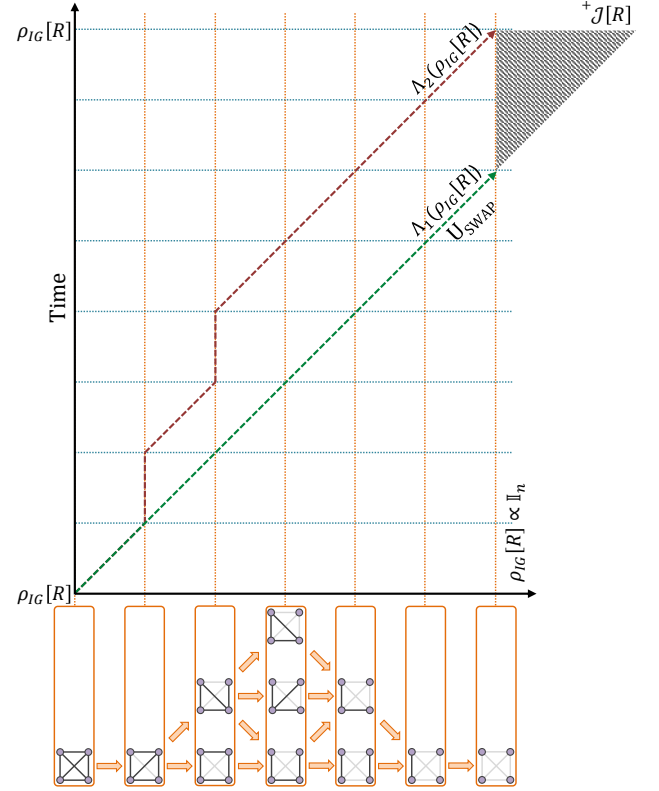


FIG. 9. A Penrose diagram representing the quantum circuit complexity for the evolution of a quantum state, which is related to a quantum circuit  $\rho_{IG}$  (for the sake of simplicity, we choose the state  $\rho_{IG}$  to be derived from the  $K_4$  graph, but one can choose other examples). It is possible to generate different quantum complexities by adding different amounts and orderings of SWAP gates to the circuit as we approach the event horizon of a black hole (shown as a shaded triangle). Here, the connectivity limitations of the CG capture the role of the background spacetime geometry [89], as both determine the ease by which certain operations can be performed. The SWAP uncomplexity, as it ignores the effects of time ordering and the amount of qubit-qubit interaction present, can be associated with the null lightlike geodesic  ${}^+J[R]$ , shown as a green dotted line. Below this arrow, the bottom-right part of the diagram represents possible states that are inaccessible to us, given the restrictions of the coupling graph, as well as the operations available to us (SWAP gates, in our case).

a given set represents a unique spectral signature which can be shared by multiple four-node subgraphs. The vertical axis depicts the evolution of time, and is known as the *null time geodesic*, under which the set of *trivial time-ordered gate operations* (i.e. idling, which in our simplified picture, is noiseless) evolve  $\rho_{IG}$  from point  $R$  to the same later state. Here, the trivial minimal SWAP gate count for the QCMP is represented, under which no SWAP gates are ever applied in order to adapt the quantum circuit to the device and its connectivity restrictions; in effect, the state is left to freely evolve for an infinite amount of time, with no regards to gate operations.

Conversely, the red dotted line represents possible spacetime evolutions arising from the application of distinct in-

stances of time-ordered quantum operations  $\Lambda_1(\cdot)$  (which in this case are insertions of SWAP gates). In this way, every trajectory on the diagram can be associated with a given SWAP uncomplexity from a sequence of quantum operations. The possible endpoints of the quantum circuit are shown along the shaded triangle in dark gray, which represents  $\rho_{\text{IG}} = \mathbb{I}_n$ , i.e. the state of maximal circuit complexity, a maximally mixed state.

Furthermore, erasure transformations on the original quantum circuit proceed according to restrictions dictated by the background geometry (which in our present case is analogous to the CG connectivity). Evolution commences at a spacetime point  $R$ . The green dotted line traces out the *lightlike null geodesic* (i.e. future lightcone)  $^+ \mathcal{J}[R]$ . This geodesic signifies the SWAP uncomplexity, which is the path that the state takes under the minimal set of causally-indefinite operations such that we approach the maximally-mixed state in minimal time. As we solve for the SWAP uncomplexity, without consideration of time ordering and as dictated by the thermodynamic path length calculable via the Fisher information metric [71, 91], we can interpret our bound as the *lightcone evolution* of our initial state  $\rho_{\text{IG}}$  towards the event horizon of a black hole (shown as the shaded triangle). Previous work has already alluded to the concept of optimization over thermodynamic distance [77, 92]; as such, our results point to a natural and reasonable extension of this trend for the quantum circuit mapping problem.

Taking stock, we would then expect that any realistic quantum compiler which takes into account time ordering and finite qubit-qubit interactions per unit of time slicing to be limited by the lightlike null geodesic. Indeed, surpassing the lightlike null geodesic would introduce operations which are not inside of the lightcone, giving access to the uncomputable region to the bottom-right. Such trajectories could be made possible using a larger set of routing resources, such as teleportation [60, 61]. On the other hand, the SWAP uncomplexity bound implies an *indefinite causal order*, which would give rise to superpositions of quantum gates that are executed in tandem [62, 63].

As we stated earlier, we can alternatively consider the shaded triangle in Figure 9 as the event horizon into a black hole. Indeed, Equation 15 gives rise to a new perspective for the QCMP, due to its apparent relation with quantum uncomplexity [42, 43]. Consider a benign black hole scenario in which the black hole itself can only erase information from a density matrix in accordance with only certain SWAP gates from some constrained architecture (i.e., the black hole itself is described with respect to a background geometry, which constrains which operations can be performed). As black holes are known to be the fastest information scramblers in nature [93], the QCMP can be viewed through the lens of a scrambling process, yielding the most-efficient method to maximally mix the information of the IG density matrix, at a given  $\beta$  value. This process exemplifies the traits of a quantum resource theory and we have shown that the quantity  $U_{\text{SWAP}}$  can in fact be optimized for using our technique.

As a counterexample, consider a hypothetical quantum compiler which could surpass  $U_{\text{SWAP}}$ . One of the main as-

sumptions that we utilize in our formulation above is that possible interactions can occur only if a subsystem interaction between qubits exists in the density matrix picture; intrinsically, moving outside the region embellished by the future lightlike geodesic corresponds to new operations which must be taken into account. One simple example lies in *teleportation-based* quantum-circuit mapping, which can be used between CG qubits which do not share a subsystem interaction, and can allow for a smaller quantum circuit complexity [60]. One may suspect that architectures in the future may benefit from such on-chip teleportation procedures, as work has shown that speedups exist over classical SWAP methods for exchanging distant qubits [32, 60, 61], albeit with larger circuit and entanglement overhead.

Finally, we close this section by discussing the  $\beta$  parameter in more detail. For the vast majority of our results (approximately  $\sim 97\%$ , as shown in Figure 6), the  $\beta$  values yielding the SWAP uncomplexity for an IG/CG pair coincide with the *high-temperature regime* noted in [78]. Indeed, it was shown there that the high-temperature regime allows for optimization of the quantum relative entropy for density matrices contrived from complex networks. The main interpretation provided in [78] is that the parameter  $\beta$  controls the diffusion of information about the graph neighborhood to other vertices. Conversely, if we take the  $\beta \mapsto 0$  limit, diffusion over the vertices of the graph is limited, and therefore, only information about the degrees of links is conferred. This trait is known to exhibit a first-order linear dependency in the adjacency matrix, and as such, the tendency for information to diffuse over the network becomes uniform. As we can see from Figure 6, less than 3% of our benchmarks do not fall within the high-temperature  $\beta$  range described in [78] (shown in red). Those outliers, however, can be explained with the triviality of the correct  $\beta$  search process, which was particularly based on sweeping over a range of values between  $10^{-5} - 10^5$ . One future direction, therefore, is to devise more efficient schemes for finding the optimal  $\beta$  value, guaranteeing a minimal bound in less computation time. One could imagine that such a goal could be completed by use of a gradient optimization method, but we leave such exploration to future work.

## VIII. CONCLUSIONS & OUTLOOK

The QCMP itself has been described using several approaches from computer science, many of which have allowed for the development of entirely new strategies for solving the problem. Our contribution here serves a different purpose. At the level of theoretical physics, quantum information theory, and information geometry, we solve a simplified subproblem of the QCMP. We have shown that solving this subproblem quantifies a minimal bound, underlying the full QCMP. At the limit where this bound is applicable, we assume implicitly that: the quantum device is noiseless; the two-qubit gate interactions given by the device can be performed with an indefinite causal order; and that any number of two-qubit interactions can be performed in tandem within one unit time slice. Our conceptualization of the QCMP provides, to our



knowledge, the first instance of a solvable lower bound for the SWAP gate count when adapting a quantum circuit to a connectivity-restricted processor. The SWAP uncomplexity was derived using tools from graph theory and quantum information theory, using insights from quantum resource theory and quantum circuit complexity. Potential applications of uncomplexity for quantum machine learning are discussed in [94]. To the best of our knowledge, this work represents *the first demonstration of an application of the concept of quantum circuit uncomplexity to the realm of practical quantum information processing*.

Our purpose for deriving the bound has therefore been to inform and to create a meaningful method of comparison between quantum compilers and strategies for solving the full QCMP. This goal has been accomplished in several key ways. Firstly, the SWAP uncomplexity sheds light onto the physical nature of the QCMP using information geometry, as well as theoretical physics. We have systematically shown that the concept of SWAP uncomplexity provides a minimal SWAP gate count for the full QCMP via considerations of the thermodynamic length and Fisher information metric, providing strong analytical arguments to supplant the empirical results obtained in Section VI. Therefore, the use of SWAP uncomplexity as a metric for routing efficiency is pragmatic and justified, and can be used to quantify and compare routing strategies, as well as helping to inform architectural decisions by quantum architects and processor designers.

Of independent interest may be the qubit-assignment algorithm which was designed to aid in the calculation of the SWAP uncomplexity. This algorithm, grounded as a graph similarity search, inspects distinct  $n$ -qubit partitions of a given coupling graph, and returns the most-similar resultant to the interaction graph provided. Employing this method has enabled us to map circuits with up to 16 qubits onto devices with up to 72 physical qubits. For larger circuits, we devised an alternative approach. The initial placement precedes the minimal SWAP gate count solution, which is further utilized for routing and minimal bound calculation. Additionally, we calculated a maximal bound by leveraging known classical graph metrics. Both of these new structures provide additional tools of interest outside of the scope of this work.

We would like to draw attention to several open problems regarding our work, as well as several future possible directions for research:

1. *Formally associating the qJSD to circuit uncomplexity.* As we stated previously, it has been shown that both the quantum circuit uncomplexity as well as the qJSD are closely related to the Fisher information and Fubini-Study metrics [42, 55, 71]. However, an exact relationship has not yet been established, as far as we are aware. Establishing this relationship on more rigorous mathematical footing could be very helpful.
2. *Improvements to the subgraph similarity search algorithm.* In this work, although our qubit-assignment algorithm outperforms the current state of the art solver [86], we were still limited by the scalability of the qubit-assignment algorithm constructed in Section V B. However, once a suitable qubit assignment is set, the calcu-

lation of  $U_{\text{SWAP}}$  can be completed in  $\mathcal{O}(n^2 + c)$  steps, as per the Birkhoff-von-Neumann algorithm [72]. A future research goal could involve making further scalability improvements to the qubit-assignment algorithm.

3. *Searching for the optimal  $\beta$  value.* In our work, we have taken a somewhat naive approach to optimizing for  $\beta$ ; however, because of the similarity of Figure 2 to a phase diagram, one may be able to use concepts from condensed matter theory [95–97] in order to devise a suitable gradient-based optimization method.
4. *Analytical expression for tightness of the SWAP uncomplexity to the brute-force solution.* We have given empirical evidence for tightness, but it still remains to define an analytical expression for how similar in general our solution is, compared to the brute-force solution proposed in [85], and how tightness scales as the size of the quantum circuit to be mapped increases in both register and depth.
5. *Extension to incorporate bridge gates and teleportation-based quantum circuit mapping.* There are other methods commonly in use, in addition to the SWAP gate, for conforming a quantum circuit to hardware. Our approach is extendable for the Bridge gates mentioned in [98–102], as well as the quantum teleportation-based protocols of [32, 60, 61, 103].
6. *Extension for quantum error correction codes, in particular syndrome extraction circuits.* It is well-known that various *fault-tolerance* protocols are required in order to ensure that quantum error correction codes function up to their full code distance [104–115]. As our bound constitutes a non-trivial resource requirement, it may be useful to adapt fault-tolerance protocols further to the setting of quantum compilation, in which an error correction code is adapted to a device not specifically designed for a particular code family [116, 117].
7. *Extension for entanglement/qubit routing in quantum communications networks and modular architectures.* Several other extensions may be possible as well, including those allowing for bounds on the QCMP for modular scenarios [118] as well as for *entanglement distribution* in noisy quantum networks [119].

Finally, we remark that the problem of assessing similarities between two complex networks is a problem spanning many disciplines. Indeed, our work follows recent trends of utilizing quantum information theory and statistical mechanics to study complex networks [39, 40, 44, 78]. As the task of comparing the distance between graphs appears in many different areas of science [65, 120], we expect the implications of our work to stretch beyond the realm of quantum information science.

## IX. SOFTWARE AVAILABILITY

The software developed for this project is available at <https://github.com/QML-Group/QCMP-complexity-bound>.

## X. ACKNOWLEDGEMENTS

We thank Kenneth Goodenough, Hans van Someren, Pablo le Henaff, Luise Prielinger, David Elkouss, and Tariq Bontekoe for insightful discussions and useful manuscript feedback. MS, MB, and SF are grateful for financial support from Intel. CGA acknowledges support from Spanish Ministerio de Ciencia e Innovación and European ERDF under grant PID2021-123627OB-C51. CGA also acknowledges support from the QuantERA grant EQUIP with the grant number PCI2022-133004, funded by Agencia Estatal de Investigación, Ministerio de Ciencia e Innovación, Gobierno de España, MCIN/AEI/10.13039/501100011033, and by the European Union “NextGenerationEU/PRTR. AS acknowledges funding from the Dutch Research Council (NWO) through the

project “QuTech Part III Application-based research” (project no. 601.QT.001 Part III-C—NISQ).

## XI. AUTHOR CONTRIBUTIONS

MS, AS, and SS developed the theoretical framework and formalism. MB, SS, and AS developed the numerical algorithm based on the framework and implemented all numerical simulations. MB developed the subgraph isomorphism qubit-assignment algorithm. Part of this work was conducted during the Master thesis for SS, and was supervised by MS, MB, and SF. CA and SF supervised and coordinated the project, and provided guidance during the writing process.

- 
- [1] M. Nielsen and I. Chuang, *Quantum Computation and Quantum Information*, ISBN 978-1-107-00217-3 (Cambridge University Press, Cambridge, UK, 2010).
- [2] J. Preskill, Quantum computing in the nisq era and beyond, *Quantum* **2**, 79 (2018).
- [3] C. Hempel, C. Maier, J. Romero, J. McClean, T. Monz, H. Shen, P. Jurcevic, B. P. Lanyon, P. Love, R. Babbush, A. Aspuru-Guzik, R. Blatt, and C. F. Roos, Quantum chemistry calculations on a trapped-ion quantum simulator, *Phys. Rev. X* **8**, 031022 (2018).
- [4] P. J. J. O’Malley, R. Babbush, I. D. Kivlichan, J. Romero, J. R. McClean, R. Barends, J. Kelly, P. Roushan, A. Tranter, N. Ding, B. Campbell, Y. Chen, Z. Chen, B. Chiaro, A. Dunsworth, A. G. Fowler, E. Jeffrey, E. Lucero, A. Megrant, J. Y. Mutus, M. Neeley, C. Neill, C. Quintana, D. Sank, A. Vainsencher, J. Wenner, T. C. White, P. V. Coveney, P. J. Love, H. Neven, A. Aspuru-Guzik, and J. M. Martinis, Scalable quantum simulation of molecular energies, *Phys. Rev. X* **6**, 031007 (2016).
- [5] D. G. Cory, M. D. Price, W. Maas, E. Knill, R. Laflamme, W. H. Zurek, T. F. Havel, and S. S. Somaroo, Experimental quantum error correction, *Phys. Rev. Lett.* **81**, 2152 (1998).
- [6] J. Chiaverini, D. Leibfried, T. Schaetz, M. D. Barrett, R. Blakestad, J. Britton, W. M. Itano, J. D. Jost, E. Knill, C. Langer, *et al.*, Realization of quantum error correction, *Nature* **432**, 602 (2004).
- [7] B. M. Terhal, Quantum error correction for quantum memories, *Reviews of Modern Physics* **87**, 307 (2015).
- [8] P. Murali, N. M. Linke, M. Martonosi, A. J. Abhari, N. H. Nguyen, and C. H. Alderete, Full-stack, real-system quantum computer studies: Architectural comparisons and design insights, in *Proceedings of the 46th International Symposium on Computer Architecture* (2019) pp. 527–540.
- [9] M. Bandic, S. Feld, and C. G. Almudever, Full-stack quantum computing systems in the nisq era: algorithm-driven and hardware-aware compilation techniques, in *2022 Design, Automation & Test in Europe Conference & Exhibition (DATE)* (IEEE, 2022) pp. 1–6.
- [10] K. Bertels, A. Sarkar, T. Hubregtsen, M. Serrao, A. Moudden, A. Yadav, A. Krol, I. Ashraf, and C. G. Almudever, Quantum computer architecture toward full-stack quantum accelerators, *IEEE Transactions on Quantum Engineering* **1**, 1 (2020).
- [11] M. Bandic, H. Zarein, E. Alarcon, and C. G. Almudever, On structured design space exploration for mapping of quantum algorithms, in *2020 XXXV conference on design of circuits and integrated systems (DCIS)* (IEEE, 2020) pp. 1–6.
- [12] G. Li, Y. Ding, and Y. Xie, Tackling the qubit mapping problem for nisq-era quantum devices, in *Proceedings of the Twenty-Fourth International Conference on Architectural Support for Programming Languages and Operating Systems, ASPLOS ’19* (Association for Computing Machinery, New York, NY, USA, 2019) p. 1001–1014.
- [13] M. Y. Siraichi, V. F. d. Santos, C. Collange, and F. M. Q. Pereira, Qubit allocation, in *Proceedings of the 2018 International Symposium on Code Generation and Optimization, CGO 2018* (Association for Computing Machinery, New York, NY, USA, 2018) p. 113–125.
- [14] A. Cowtan, S. Dilkes, R. Duncan, A. Krajenbrink, W. Simmons, and S. Sivarajah, On the qubit routing problem, in *14th Conference on the Theory of Quantum Computation, Communication and Cryptography (TQC 2019)* (Schloss Dagstuhl-Leibniz-Zentrum fuer Informatik, 2019).
- [15] N. Alon, F. R. Chung, and R. L. Graham, Routing permutations on graphs via matchings, in *Proceedings of the twenty-fifth annual ACM symposium on Theory of Computing* (1993) pp. 583–591.
- [16] A. Paler, A. Zulehner, and R. Wille, Nisq circuit compilation is the travelling salesman problem on a torus, *Quantum Science and Technology* **6**, 025016 (2021).
- [17] T. Miltzow, L. Narins, Y. Okamoto, G. Rote, A. Thomas, and T. Uno, Approximation and hardness for token swapping, arXiv preprint arXiv:1602.05150 (2016).
- [18] F. Wagner, A. Bärmann, F. Liers, and M. Weissenböck, Improving quantum computation by optimized qubit routing, *Journal of Optimization Theory and Applications*, 1 (2023).
- [19] P. Murali, J. M. Baker, A. Javadi-Abhari, F. T. Chong, and M. Martonosi, Noise-adaptive compiler mappings for noisy intermediate-scale quantum computers, in *International Conference on Architectural Support for Programming Languages and Operating Systems* (2019) pp. 1015–1029.
- [20] S. S. Tannu and M. K. Qureshi, Not all qubits are created equal: A case for variability-aware policies for NISQ-era quantum computers, in *International Conference on Architectural Support for Programming Languages and Operating Systems* (2019) pp. 987–999.

- [21] G. LI, Y. Ding, and Y. Xie, Towards efficient superconducting quantum processor architecture design, in *Proceedings of the Twenty-Fifth International Conference on Architectural Support for Programming Languages and Operating Systems* (2020) pp. 1031–1045.
- [22] A. Zulehner, A. Paler, and R. Wille, An efficient methodology for mapping quantum circuits to the IBM QX architectures, *IEEE Transactions on Computer-Aided Design of Integrated Circuits and Systems* (2018).
- [23] D. Venturelli, M. Do, B. O’Gorman, J. Frank, E. Rieffel, K. E. C. Booth, T. Nguyen, P. Narayan, and S. Nanda, Quantum circuit compilation: An emerging application for automated reasoning, in *Scheduling and Planning Applications Workshop* (2019).
- [24] L. Lao, B. van Wee, I. Ashraf, J. van Someren, N. Khammassi, K. Bertels, and C. Almudever, Mapping of lattice surgery-based quantum circuits on surface code architectures, *Quantum Science and Technology* **4**, 015005 (2019).
- [25] L. Lao, D. M. Manzano, H. van Someren, I. Ashraf, and C. G. Almudever, Mapping of quantum circuits onto nisq superconducting processors, arXiv preprint arXiv:1908.04226 (2019).
- [26] S. Herbert and A. Sengupta, Using reinforcement learning to find efficient qubit routing policies for deployment in near-term quantum computers, arXiv:1812.11619 (2018).
- [27] A. Lye, R. Wille, and R. Drechsler, Determining the minimal number of swap gates for multi-dimensional nearest neighbor quantum circuits, in *Asia and South Pacific Design Automation Conference* (2015) pp. 178–183.
- [28] S. Li, X. Zhou, and Y. Feng, Qubit mapping based on subgraph isomorphism and filtered depth-limited search, *IEEE Transactions on Computers* **70**, 1777 (2020).
- [29] A. Biuki, N. Mohammadzadeh, R. Wille, and S. Sargaran, Exact mapping of quantum circuit partitions to building blocks of the saqip architecture, in *2022 IEEE Computer Society Annual Symposium on VLSI (ISVLSI)* (IEEE, 2022) pp. 402–405.
- [30] A. Molavi, A. Xu, M. Diges, L. Pick, S. Tannu, and A. Albarghouthi, Qubit mapping and routing via maxsat, in *2022 55th IEEE/ACM International Symposium on Microarchitecture (MICRO)* (IEEE, 2022) pp. 1078–1091.
- [31] L. Moro, M. G. Paris, M. Restelli, and E. Prati, Quantum compiling by deep reinforcement learning, *Communications Physics* **4**, 178 (2021).
- [32] D. Devulapalli, E. Schoute, A. Bapat, A. M. Childs, and A. V. Gorshkov, Quantum routing with teleportation (2022), arXiv:2204.04185 [quant-ph].
- [33] S. Upadhyay, A. A. Saki, R. O. Topaloglu, and S. Ghosh, A shuttle-efficient qubit mapper for trapped-ion quantum computers, in *Proceedings of the Great Lakes Symposium on VLSI 2022* (2022) pp. 305–308.
- [34] N. Nottingham, M. A. Perlin, R. White, H. Bernien, F. T. Chong, and J. M. Baker, Decomposing and routing quantum circuits under constraints for neutral atom architectures, arXiv preprint arXiv:2307.14996 (2023).
- [35] M. M. Wilde, *Quantum Information Theory*, 2nd ed. (Cambridge University Press, 2017).
- [36] J. Watrous, *The theory of quantum information* (Cambridge university press, 2018).
- [37] A. Di Meglio, K. Jansen, I. Tavernelli, C. Alexandrou, S. Arunachalam, C. W. Bauer, K. Borras, S. Carrazza, A. Crippa, V. Croft, *et al.*, Quantum computing for high-energy physics: State of the art and challenges. summary of the qc4hep working group, arXiv preprint arXiv:2307.03236 (2023).
- [38] D. Harlow, Jerusalem lectures on black holes and quantum information, *Rev. Mod. Phys.* **88**, 015002 (2016).
- [39] M. De Domenico and J. Biamonte, Spectral entropies as information-theoretic tools for complex network comparison, *Physical Review X* **6**, 10.1103/physrevx.6.041062 (2016).
- [40] M. Faccin and J. Biamonte, Complex networks from classical to quantum, *Nature Communications Physics* **2**, 10.1038/s42005-019-0152-6 (2019).
- [41] S. L. Braunstein, S. Ghosh, and S. Severini, The laplacian of a graph as a density matrix: A basic combinatorial approach to separability of mixed states, *Annals of Combinatorics* **10**, 291–317 (2006).
- [42] A. R. Brown and L. Susskind, Second law of quantum complexity, *Phys. Rev. D* **97**, 086015 (2018).
- [43] N. Yunger Halpern, N. B. T. Kothakonda, J. Haferkamp, A. Munson, J. Eisert, and P. Faist, Resource theory of quantum uncomplexity, *Phys. Rev. A* **106**, 062417 (2022).
- [44] A. Glos, A. Krawiec, and L. Pawela, Asymptotic entropy of the gibbs state of complex networks, *Scientific Reports* **11**, 1 (2021).
- [45] J. Briët and P. Harremoës, Properties of classical and quantum jensen-shannon divergence, *Physical Review A* **79**, 10.1103/physreva.79.052311 (2009).
- [46] P. W. Lamberti, A. P. Majtey, A. Borras, M. Casas, and A. Plastino, Metric character of the quantum jensen-shannon divergence, *Physical Review A* **77**, 10.1103/physreva.77.052311 (2008).
- [47] M. Wolf, *Quantum channels and operations: A guided tour* (2012).
- [48] M. Christandl, *Quantum information theory lecture notes* (2018).
- [49] M. Nielsen, *An introduction to majorization and its applications to quantum mechanics: Lecture notes* (2002).
- [50] M. A. Steinberg, S. Feld, C. G. Almudever, M. Marthaler, and J.-M. Reiner, Topological-graph dependencies and scaling properties of a heuristic qubit-assignment algorithm, *IEEE Transactions on Quantum Engineering* **3**, 1 (2022).
- [51] M. Y. Siraichi, V. F. d. Santos, C. Collange, and F. M. Q. Pereira, Qubit allocation, in *Proceedings of the 2018 International Symposium on Code Generation and Optimization* (2018) pp. 113–125.
- [52] M. Y. Siraichi, V. F. d. Santos, C. Collange, and F. M. Q. Pereira, Qubit allocation as a combination of subgraph isomorphism and token swapping, *Proceedings of the ACM on Programming Languages* **3**, 1 (2019).
- [53] M. Bandic, C. G. Almudever, and S. Feld, Interaction graph-based characterization of quantum benchmarks for improving quantum circuit mapping techniques, *Quantum Machine Intelligence* **5**, 40 (2023).
- [54] T. Sagawa, Entropy, divergence, and majorization in classical and quantum thermodynamics (2020), arXiv:2007.09974 [quant-ph].
- [55] I. Bengtsson and K. Życzkowski, *Geometry of quantum states: an introduction to quantum entanglement* (Cambridge university press, 2017).
- [56] L. A. Zager and G. C. Verghese, Graph similarity scoring and matching, *Applied mathematics letters* **21**, 86 (2008).
- [57] D. Koutra, A. Parikh, A. Ramdas, and J. Xiang, Algorithms for graph similarity and subgraph matching, in *Proc. Ecol. inference conf*, Vol. 17 (Citeseer, 2011).
- [58] K. Samanvi and N. Sivadasan, Subgraph similarity search in large graphs, arXiv preprint arXiv:1512.05256 (2015).
- [59] S. Niu and A. Todri-Sanial, Multi-programming cross platform benchmarking for quantum computing hardware, arXiv



- preprint arXiv:2206.03144 (2022).
- [60] A. Bapat, A. M. Childs, A. V. Gorshkov, and E. Schoute, Advantages and limitations of quantum routing, *PRX Quantum* **4**, 010313 (2023).
- [61] S. Hillmich, A. Zulehner, and R. Wille, Exploiting quantum teleportation in quantum circuit mapping, in *Proceedings of the 26th Asia and South Pacific Design Automation Conference*, ASPDAC '21 (Association for Computing Machinery, New York, NY, USA, 2021) p. 792–797.
- [62] Č. Brukner, Quantum causality, *Nature Physics* **10**, 259 (2014).
- [63] K. Goswami and J. Romero, Experiments on quantum causality, *AVS Quantum Science* **2** (2020).
- [64] J. J. Sakurai and E. D. Commins, *Modern quantum mechanics*, revised edition (1995).
- [65] S. H. Strogatz, Exploring complex networks, *nature* **410**, 268 (2001).
- [66] F. Green, Review of handbook of graph theory, combinatorial optimization, and algorithms, *SIGACT News* **50**, 6–11 (2019).
- [67] C. Godsil and G. F. Royle, *Algebraic graph theory*, Vol. 207 (Springer Science & Business Media, 2001).
- [68] A. P. Majtey, P. W. Lamberti, and D. P. Prato, Jensen-shannon divergence as a measure of distinguishability between mixed quantum states, *Phys. Rev. A* **72**, 052310 (2005).
- [69] M. De Domenico, V. Nicosia, A. Arenas, and V. Latora, Structural reducibility of multilayer networks, *Nature communications* **6**, 6864 (2015).
- [70] L. Rossi, A. Torsello, and E. R. Hancock, Attributed graph similarity from the quantum jensen-shannon divergence, in *Similarity-Based Pattern Recognition: Second International Workshop, SIMBAD 2013, York, UK, July 3-5, 2013. Proceedings 2* (Springer, 2013) pp. 204–218.
- [71] G. E. Crooks, Measuring thermodynamic length, *Phys. Rev. Lett.* **99**, 100602 (2007).
- [72] D. M. Johnson, A. Dulmage, and N. Mendelsohn, On an algorithm of g. birkhoff concerning doubly stochastic matrices, *Canadian Mathematical Bulletin* **3**, 237 (1960).
- [73] P. Virtanen, R. Gommers, T. E. Oliphant, M. Haberland, T. Reddy, D. Cournapeau, E. Burovski, P. Peterson, W. Weckesser, J. Bright, S. J. van der Walt, M. Brett, J. Wilson, K. J. Millman, N. Mayorov, A. R. J. Nelson, E. Jones, R. Kern, E. Larson, C. J. Carey, Í. Polat, Y. Feng, E. W. Moore, J. VanderPlas, D. Laxalde, J. Perktold, R. Cimrman, I. Henriksen, E. A. Quintero, C. R. Harris, A. M. Archibald, A. H. Ribeiro, F. Pedregosa, P. van Mulbregt, and SciPy 1.0 Contributors, SciPy 1.0: Fundamental Algorithms for Scientific Computing in Python, *Nature Methods* **17**, 261 (2020).
- [74] R. Cheng, Quantum geometric tensor (fubini-study metric) in simple quantum system: A pedagogical introduction, arXiv preprint arXiv:1012.1337 (2010).
- [75] F. Benatti and H. Narnhofer, Entropy behaviour under completely positive maps, *letters in mathematical physics* **15**, 325 (1988).
- [76] E. Chitambar and G. Gour, Quantum resource theories, *Rev. Mod. Phys.* **91**, 025001 (2019).
- [77] P. Abiuso, H. J. Miller, M. Perarnau-Llobet, and M. Scandi, Geometric optimisation of quantum thermodynamic processes, *Entropy* **22**, 1076 (2020).
- [78] C. Nicolini, V. Vlasov, and A. Bifone, Thermodynamics of network model fitting with spectral entropies, *Phys. Rev. E* **98**, 022322 (2018).
- [79] T. Bahreini and N. Mohammadzadeh, An MINLP model for scheduling and placement of quantum circuits with a heuristic solution approach, *Journal on Emerging Technologies in Computing* **12**, 29 (2015).
- [80] G. Li *et al.*, Tackling the qubit mapping problem for NISQ-era quantum devices, in *International Conference on Architectural Support for Programming Languages and Operating Systems* (2019) pp. 1001–1014.
- [81] H. Jiang, Y. Deng, and M. Xu, Quantum circuit transformation based on tabu search, arXiv preprint arXiv:2104.05214 (2021).
- [82] T. Peham, L. Burgholzer, and R. Wille, On optimal subarchitectures for quantum circuit mapping, *ACM Transactions on Quantum Computing* **4**, 1 (2023).
- [83] L. P. Cordella, P. Foggia, C. Sansone, and M. Vento, A (sub) graph isomorphism algorithm for matching large graphs, *IEEE transactions on pattern analysis and machine intelligence* **26**, 1367 (2004).
- [84] Qiskit contributors, *Qiskit: An open-source framework for quantum computing* (2023).
- [85] A. Lye, R. Wille, and R. Drechsler, Determining the minimal number of swap gates for multi-dimensional nearest neighbor quantum circuits, in *The 20th Asia and South Pacific Design Automation Conference* (2015) pp. 178–183.
- [86] A. Shafaei, M. Saeedi, and M. Pedram, Qubit placement to minimize communication overhead in 2d quantum architectures, in *2014 19th Asia and South Pacific Design Automation Conference (ASP-DAC)* (2014) pp. 495–500.
- [87] D. Freedman, R. Pisani, and R. Purves, *Statistics* (international student edition), Pisani, R. Purves, 4th edn. WW Norton & Company, New York (2007).
- [88] L. Lao, H. van Someren, I. Ashraf, and C. G. Almudever, Timing and resource-aware mapping of quantum circuits to superconducting processors, *IEEE Transactions on Computer-Aided Design of Integrated Circuits and Systems* (2021).
- [89] S. M. Carroll, *Spacetime and geometry* (Cambridge University Press, 2019).
- [90] R. Penrose, Asymptotic properties of fields and space-times, *Phys. Rev. Lett.* **10**, 66 (1963).
- [91] M. Scandi and M. Perarnau-Llobet, Thermodynamic length in open quantum systems, *Quantum* **3**, 197 (2019).
- [92] S. Ito, Stochastic thermodynamic interpretation of information geometry, *Phys. Rev. Lett.* **121**, 030605 (2018).
- [93] Y. Sekino and L. Susskind, Fast scramblers, *Journal of High Energy Physics* **2008**, 065 (2008).
- [94] A. Sarkar, *Applications of Quantum Computation and Algorithmic Information: for Causal Modeling in Genomics and Reinforcement Learning*, Phd thesis, Delft University of Technology (2022).
- [95] N. Goldenfeld, *Lectures on phase transitions and the renormalization group* (CRC Press, 2018).
- [96] G. R. Brightwell and P. Winkler, Graph homomorphisms and phase transitions, *Journal of combinatorial theory, series B* **77**, 221 (1999).
- [97] S. N. Dorogovtsev, A. V. Goltsev, and J. F. F. Mendes, Critical phenomena in complex networks, *Rev. Mod. Phys.* **80**, 1275 (2008).
- [98] S. Niu, A. Suau, G. Staffelbach, and A. Todri-Sanial, A hardware-aware heuristic for the qubit mapping problem in the nisq era, *IEEE Transactions on Quantum Engineering* **1**, 1 (2020).
- [99] T. Itoko, R. Raymond, T. Imamichi, and A. Matsuo, Optimization of quantum circuit mapping using gate transformation and commutation, *Integration* **70**, 43 (2020).
- [100] S. Park, D. Kim, M. Kweon, J.-Y. Sim, and S. Kang, A fast and scalable qubit-mapping method for noisy intermediate-scale quantum computers, in *Proceedings of the 59th ACM/IEEE*



- Design Automation Conference*, DAC '22 (Association for Computing Machinery, New York, NY, USA, 2022) p. 13–18.
- [101] J. Liu, E. Younis, M. Weiden, P. Hovland, J. Kubitowicz, and C. Iancu, Tackling the qubit mapping problem with permutation-aware synthesis, arXiv preprint arXiv:2305.02939 (2023).
- [102] S. Park, D. Kim, J.-Y. Sim, and S. Kang, Mcqa: Multi-constraint qubit allocation for near-ftqc device, in *Proceedings of the 41st IEEE/ACM International Conference on Computer-Aided Design*, ICCAD '22 (Association for Computing Machinery, New York, NY, USA, 2022).
- [103] S. Hillmich, A. Zulehner, and R. Wille, Exploiting quantum teleportation in quantum circuit mapping, in *2021 26th Asia and South Pacific Design Automation Conference (ASP-DAC)* (IEEE, 2021) pp. 792–797.
- [104] J. Preskill, Reliable quantum computers, *Proceedings of the Royal Society of London. Series A: Mathematical, Physical and Engineering Sciences* **454**, 385 (1998).
- [105] D. Bhatnagar, M. Steinberg, D. Elkouss, C. G. Almudever, and S. Feld, Low-depth flag-style syndrome extraction for small quantum error-correction codes, in *2023 IEEE International Conference on Quantum Computing and Engineering (QCE)*, Vol. 01 (2023) pp. 63–69.
- [106] D. Gottesman, An introduction to quantum error correction and fault-tolerant quantum computation, in *Quantum information science and its contributions to mathematics, Proceedings of Symposia in Applied Mathematics*, Vol. 68 (2010) pp. 13–58.
- [107] D. Gottesman, Theory of fault-tolerant quantum computation, *Phys. Rev. A* **57**, 127 (1998).
- [108] C. Chamberland and M. E. Beverland, Flag fault-tolerant error correction with arbitrary distance codes, *Quantum* **2**, 53 (2018).
- [109] A. M. Steane, Overhead and noise threshold of fault-tolerant quantum error correction, *Phys. Rev. A* **68**, 042322 (2003).
- [110] A. W. Cross, D. P. DiVincenzo, and B. M. Terhal, A comparative code study for quantum fault-tolerance, arXiv preprint arXiv:0711.1556 (2007).
- [111] E. T. Campbell, B. M. Terhal, and C. Vuillot, Roads towards fault-tolerant universal quantum computation, *Nature* **549**, 172 (2017).
- [112] P. Aliferis, D. Gottesman, and J. Preskill, Quantum accuracy threshold for concatenated distance-3 codes, arXiv preprint quant-ph/0504218 (2005).
- [113] D. Aharonov and M. Ben-Or, Fault-tolerant quantum computation with constant error, in *Proceedings of the twenty-ninth annual ACM symposium on Theory of computing* (1997) pp. 176–188.
- [114] E. Knill, Quantum computing with realistically noisy devices, *Nature* **434**, 39 (2005).
- [115] R. Chao and B. W. Reichardt, Quantum error correction with only two extra qubits, *Phys. Rev. Lett.* **121**, 050502 (2018).
- [116] D. A. Lidar and T. A. Brun, *Quantum error correction* (Cambridge university press, 2013).
- [117] L. Lao and C. G. Almudever, Fault-tolerant quantum error correction on near-term quantum processors using flag and bridge qubits, *Phys. Rev. A* **101**, 032333 (2020).
- [118] M. Bandic, L. Prielinger, J. Nüßlein, A. Ovide, S. Rodrigo, S. Abadal, H. van Someren, G. Vardoyan, E. Alarcon, C. G. Almudever, *et al.*, Mapping quantum circuits to modular architectures with qubo, arXiv preprint arXiv:2305.06687 (2023).
- [119] M. Pant, H. Krovi, D. Towsley, L. Tassiulas, L. Jiang, P. Basu, D. Englund, and S. Guha, Routing entanglement in the quantum internet, *npj Quantum Information* **5**, 25 (2019).
- [120] R. Albert and A.-L. Barabási, Statistical mechanics of complex networks, *Rev. Mod. Phys.* **74**, 47 (2002).
- [121] P. F. C. Sansone, M. Vento, L. Cordella, P. Foggia, C. Sansone, and M. Vento, An improved algorithm for matching large graphs, in *Proc. of the 3rd IAPR-TC-15 International Workshop on Graph-based Representations*, Vol. 57 (2001).
- [122] V. Bonnici, R. Giugno, A. Pulvirenti, D. Shasha, and A. Ferro, A subgraph isomorphism algorithm and its application to biochemical data, *BMC bioinformatics* **14**, 1 (2013).
- [123] C. Solnon, Alldifferent-based filtering for subgraph isomorphism, *Artificial Intelligence* **174**, 850 (2010).
- [124] J. R. Ullmann, Bit-vector algorithms for binary constraint satisfaction and subgraph isomorphism, *Journal of Experimental Algorithmics (JEA)* **15**, 1 (2011).
- [125] R. M. Roth, Introduction to coding theory, *IET Communications* **47**, 4 (2006).
- [126] Z. Abu-Aisheh, R. Raveaux, J.-Y. Ramel, and P. Martineau, An exact graph edit distance algorithm for solving pattern recognition problems, in *4th International Conference on Pattern Recognition Applications and Methods 2015* (2015).
- [127] P. H. Sellers, On the theory and computation of evolutionary distances, *SIAM Journal on Applied Mathematics* **26**, 787 (1974).
- [128] J. Nocedal and S. J. Wright, *Numerical optimization* (Springer, 1999).
- [129] S. J. Russell and P. Norvig, *Artificial intelligence a modern approach* (London, 2010).
- [130] J. M. Hernández and P. Van Mieghem, Classification of graph metrics, Delft University of Technology: Mekelweg, The Netherlands, 1 (2011).
- [131] A collection of quantum circuits for benchmarking quantum system software, <https://github.com/QML-Group/qbench> (2023 (accessed Jan 31, 2024)).

## Appendix A: Graph Theory

In Figure 1, the IG and CG are examples of *simple, undirected graphs* [66], with *simple* referring to a restriction of only one edge between any two vertices, and *undirected* meaning without directionality indicated by arrows. For this work, we restrict ourselves to this regime only. An example of a simple, undirected graph can be seen in Figure 1B. Here, we define a graph as an ordered-pair object  $G(E_G, V_G)$  with edge set  $E_G = \{e_{ij} | i, j \in V_G, i \neq j\}$  and vertex set  $V_G$  containing all nodes of  $G$  [67]. Additionally, we define the *adjacency matrix*  $\mathbf{A}$ , *degree matrix*  $\mathbf{D}$ , and *combinatorial graph Laplacian*  $\mathbf{L}$  from literature [39, 40]. As usual, the graph Laplacian takes on the form  $\mathbf{L} = \mathbf{D} - \mathbf{A}$ .

From here onwards, we will refer to the combinatorial graph Laplacian as simply the *graph Laplacian*. Several forms of the graph Laplacian exist in the literature [39–41, 44, 66, 67]; as such, we have opted to use the definition of the graph Laplacian which upholds the triangle inequality [39, 40]. The graph Laplacian in the current context is known to be symmetric and positive semidefinite.

Let us also define the notions of *graph isomorphism* and *homomorphisms*, as we will use these later. For two graphs  $G(E_G, V_G)$  and  $H(E_H, V_H)$  with  $|V_G| = |V_H|$ , we say that  $G$  and  $H$  are *cospectral* if they share the same eigenvalue spectrum [67]. Note that the graph Laplacian’s eigenvalue spectrum is *not sufficient* in order to determine whether or not two graphs are the same; this reason motivates us towards the treatment described in Section III and originally treated in [39, 40] with Gibbs states.

Additionally, we say that  $G$  and  $H$  are *graph homomorphic* if there exists a map  $G \mapsto H$  such that the vertex and edge connectivities of the two graphs are preserved; we represent this relation in the text as  $G \triangleq H$ . The task of determining whether or not two graphs exhibit a graph isomorphism or homomorphism is in general NP-complete [66, 67], although certain exceptions exist. If we are looking for an *embedding* of graph  $G$  onto graph  $H$  such that, for some subgraph  $H' \subseteq H$ , we have  $G \triangleq H'$ . The generalization of this problem is known as the *subgraph-isomorphism problem* (SIP). As we allow  $|V_G| \subseteq |V_H|$ , the task adds an additional layer of complexity, since we must identify a suitable subgraph for comparison; this subgraph is known as an *induced subgraph*, and is defined as a subgraph  $G' \subseteq G$  for which  $V_{G'} \subseteq V_G$  and  $E_{G'} \subseteq E_G$ .

We further remark that solving the SIP efficiently is still an active area of research, and various approaches exist for addressing it. These methods range from brute-force approaches to more sophisticated algorithms that exploit specific properties of the graphs being analyzed. Some of the most common algorithms used for solving the SIP include the Vento-Foggia algorithm (VF2) [83, 121], RI [122], The LAD (Labeled Anatomy Directed) [123] and Ullman [124] algorithms. Each algorithm has its strengths and weaknesses, and the choice depends on the specific requirements of the application. VF2 *algorithm* is a most commonly used algorithm for solving the SIP known for its speed and effectiveness. It works by maintaining a partial matching between the nodes of the pattern and

target graphs. It starts with an empty matching and gradually extends the matching by adding pairs of nodes, one from the pattern graph and one from the target graph, until a complete matching is found or it is determined that no matching exists. It has a worst-case time complexity of  $O(|V|^2 * |E|)$ , where  $|V|$  is the number of nodes in the graph and  $|E|$  is the number of edges.

If an exact isomorphism cannot be found, one must choose a subgraph known to be close to a graph isomorphism, i.e., as close to a graph homomorphism as possible. Just as for the SIP, many approaches exist for extending into the regime of subgraphs [56–58] exhibiting graph homomorphisms. Typically, one employs some graph-theoretic distance metric in order to locate the most similar subgraph [125–127].

Finally, as we will require the use of the *graph-edit distance* (GED) in Section VB, we give a brief definition of this metric. The GED itself is known as a *classical similarity measure* between two graphs  $G$  and  $H$  [66, 67]. Given a set of *graph-edit operations* (such as edge addition or edge removal in our case), one may define the GED as:

$$\text{GED}(G, H) = \min_{\{e_1 \dots e_i\} \in S_{\text{ops}(G, H)}} \sum_i c(e_i), \quad (\text{A1})$$

where  $\{e_i\} \in S_{\text{ops}(G, H)}$  represents the set of graph-edit operations along all possible graph-edit paths between graphs  $G$  and  $H$ .  $c(e_i)$  is the *cost* of the graph-edit operation. An exact algorithmic implementation of the GED usually can be found in the *A\* search algorithm*, wherein the problem of finding the minimal graph-edit cost is transformed into a *shortest-path algorithm* [128, 129]. However, in this work, we introduce an algorithm based on the depth-first GED (*DF-GED*) algorithm [126], which we detail in Section VB.

## Appendix B: Quantum Information Theory

In this section, we review some of the basics of quantum information theory which may be useful later. We refer the reader to [1, 35, 36] for a more nuanced treatise of quantum information theory.

In quantum computation and quantum information theory, the fundamental information unit is known as a *qubit*. Any pure qubit state can be represented as:

$$|\psi\rangle = \alpha |0\rangle + \beta |1\rangle, \quad (\text{B1})$$

where  $|\alpha|^2 + |\beta|^2 = 1$ . Qubits are defined in a *Hilbert space*  $\mathcal{H}$ ; these are known as *inner-product spaces* on the field of complex numbers.

Representing systems of many qubits becomes a cumbersome task when such systems are entangled with other systems. For pure quantum states, it suffices to utilize Dirac notation, but, when mixed states are involved, one conventionally uses the language of *density matrices*  $\rho$ , whose explicit form is given by:

$$\rho = \sum_j p_j |\psi\rangle \langle \psi|, \quad (\text{B2})$$

where  $p_j$  represents the probability of each pure state in the ensemble.

Density matrices exhibit several important properties for the present work. Density matrices in general are:

- Defined formally as objects  $\rho$  such that  $\rho \in \mathcal{M}_d(\mathbb{C}) \cong \mathcal{B}(\mathcal{H}^d)$ , equipped with a Hilbert-Schmidt scalar product as usual (where  $d$  is the dimension of the Hilbert space). Here,  $\mathcal{M}_d(\mathbb{C})$  represents the set of complex-valued  $d \times d$  square matrices, and  $\mathcal{B}(\mathcal{H}^d)$  is the set of bounded linear operators on a Hilbert space [47];
- Normalized, such that  $\text{Tr}(|\psi\rangle\langle\psi|) = 1$ ;
- Positive, such that  $\rho \geq 0$ ;
- Hermitian, meaning  $\rho = \rho^\dagger$ ; and
- Projectors, where  $\rho = \rho^2$ .

In quantum information theory, we customarily distinguish the amount of entanglement present in multipartite quantum systems using the *Von Neumann entropy* (VNE) [1, 49], which has the following definition:

$$\mathcal{S}(\rho) = -\text{Tr}(\rho \log \rho), \quad (\text{B3})$$

where all logarithms are of natural base. The VNE exhibits several interesting properties:

- **Permutation-invariance with respect to subsystem ordering:** that is, given a multipartite quantum state, the VNE is invariant under the specific ordering of subsystems that we choose. For example, given a state vector of five subsystems a, b, c, d, and e, we have  $\mathcal{S}(\rho) = \mathcal{S}(\sigma)$ , if  $\rho = \sum_{abcde \in \mathbb{Z}_2} |abcde\rangle\langle abcde|$ , and  $\sigma = \sum_{abcde \in \mathbb{Z}_2} |baced\rangle\langle baced|$ .
- **Unitary-transformation invariance:** a density matrix  $\rho$  is invariant under  $\mathcal{S}(\rho) = \mathcal{S}(U\rho U^\dagger)$ , where  $U$  is a unitary transformation.
- **Additivity:** the VNE is additive for independent systems. For example, for independent subsystems  $A$  and  $B$ , we have  $\mathcal{S}(\rho_A \otimes \rho_B) = \mathcal{S}(\rho_A) + \mathcal{S}(\rho_B)$ .
- **Subadditivity:** crucially, we see that a conjoined system  $AB$  has  $\mathcal{S}(\rho_{AB}) \leq \mathcal{S}(\rho_A) + \mathcal{S}(\rho_B)$ .

The task of distinguishing two quantum states can be addressed using *entropic divergences* [36, 45, 46, 49, 68, 69]. For our purposes, we define the *quantum Jensen-Shannon divergence* (qJSD) as:

$$\mathcal{D}_{\text{qJSD}}(\rho||\sigma) = \mathcal{S}\left(\frac{\rho + \sigma}{2}\right) - \frac{1}{2}(\mathcal{S}(\rho) + \mathcal{S}(\sigma)). \quad (\text{B4})$$

The quantum Jensen-Shannon divergence has several useful properties, but arguably the most important one originates from the square root of the qJSD lies in a *metric space*  $\mathcal{D}(x, y)$  for two objects  $x, y$  that we wish to distinguish. A metric space is endowed with the properties of:

- **Distance:** Let  $x, y, z$  be the elements inside a set  $X$ , then the function  $\mathcal{D} : X \times X \mapsto \mathbb{R}$  upholds  $\mathcal{D}(x, y) \geq 0$ , with the case of  $\mathcal{D} = 0$  if  $x = y$ .
- **Symmetry:** The function  $\mathcal{D}(x, y)$  also obeys  $\mathcal{D}(x, y) = \mathcal{D}(y, x)$ .
- **Adherence to the Triangle inequality:** lastly,  $\mathcal{D}(x, y) + \mathcal{D}(x, z) \geq \mathcal{D}(y, z)$ .

If these conditions are all upheld, we say that  $\mathcal{D}(\cdot, \cdot)$  is known as a *metric space* [46]. In this way, the VNE and qJSD

allow for the construction of a method to compare density matrices.

We have, until now, mainly discussed static properties of density matrices in the formalism of quantum physics. For considering *evolutions*, let us introduce the notion of a *quantum operation* (or quantum evolution) [1, 35, 36]. Succinctly, a quantum operation is a map from the space of density matrices to the space of density matrices. More formally, we define a quantum operation as a map  $\Lambda : \mathcal{M}_d(\mathbb{C}) \mapsto \mathcal{M}_d(\mathbb{C})$  that is both *linear* and *completely positive* (CP). We may additionally equip  $\Lambda(\cdot)$  with the property of *trace preservation* (TP), in which case we refer to this operation as a *quantum channel* (or *completely-positive, trace-preserving* (CPTP) map) [1, 35, 47, 48]. Finally, one may also impose *unitarity* as an extra condition.

Although there are several representations of quantum channels [47, 48], in this work we will utilize the *Kraus-operator* representation of a quantum channel, described as:

$$\Lambda(\rho) = \sum_i E_i \rho E_i^\dagger = \sigma, \quad (\text{B5})$$

where  $E_i$  represents the  $i^{\text{th}}$  term in the sum of operators and  $\sigma$  represents the output density matrix.

Measurement operations can also readily be described using the quantum-operation formalism; in the case of our work, we will utilize the case of *projective measurements*, operators  $\Pi_i$  that fulfill the relation  $\Pi_i^2 = \Pi_i$ . For representing a projective measurement in the Kraus formalism, we simply set the convention  $E_i = \sqrt{\Pi_i}$ . More information about projective measurements in quantum information theory and graph theory can be found in [1, 41].

### Appendix C: Calculating the Maximal Bound

We briefly introduce here a metric related to qubit assignment in order to approximate a maximal bound. This bound was employed in Section VI. The metric  $\mathcal{M}_{\text{SWAP}}$  involves assessing the *diameter*  $\mathbb{D}(\cdot)$  [130] of the CG subgraph  $G'_{\text{CG}}$  that is selected for qubit assignment. We then simply multiply the diameter with the amount of two-qubit gates, equivalent to the number of edges,  $|E_{\text{IG}}|$  in the circuit. This forms our approximate maximal bound for the number of SWAP gates, and takes on the following algebraic form:

$$\mathcal{M}_{\text{SWAP}}(E_{\text{IG}}, G'_{\text{CG}}) = |E_{\text{IG}}| \cdot (\mathbb{D}(G'_{\text{CG}}) - 1). \quad (\text{C1})$$

By considering the maximal distance between any two points in the chosen CG subgraph and imagining the worst-case scenario in which all the two-qubit gates are on the path between those two points, we get this maximal bound. This approach, although approximate, offers a broader perspective on the possible SWAP overhead associated with the qubit assignment, enhancing the depth and utility of our analysis. It is worth noting that, unlike the minimal bound derived in Section IV, our approach for the maximal bound involves using *weighted* IGs, taking into account the two-qubit gate depth of the underlying circuit; this makes our maximal bound specific to each benchmark.

**Appendix D: Benchmarks and quantum devices used for experiments**

TABLE I. Quantum devices used for simulations: We chose 16 of the most renowned device layouts of superconducting technology. We opted for superconducting qubits as the limit in connectivity characterizes them. The coupling graphs range in size from 5 to 72 qubits.

Quantum device	Number of qubits
IBM Athens	5
QuTech Starmon-5	5
IBM Yorktown	5
IBM Ourense	5
QuTech Surface-7	7
IBM Casablanca	7
Rigetti Agave	8
IBM Melbourne	15
Rigetti Aspen-1	16
QuTech Surface-17	17
IBM Singapore	20
IBM Johannesburg	20
IBM Tokyo	20
IBM Paris	27
IBM Rochester	53
Google Bristlecone	72



TABLE II. Benchmarks used for experiments taken from [131]. The benchmarks are characterized by different IG connectivities and range from 3 to 20 qubits.

Benchmark	Number of qubits	Number of gates	2-qubit gate %
basis_change_n3	3	79	0,126582278
fredkin_n3	3	51	0,156862745
grover_n3	3	102	0,117647059
teleportation_n3	3	20	0,1
adder_n4	4	63	0,158730159
bell_n4	4	66	0,106060606
cuccaroAdder_1b	4	83	0,204819277
q=4_s=19996_2qbf=02_1	4	20000	0,20365
q=4_s=2996_2qbf=08_1	4	3000	0,814
variational_n4	4	94	0,170212766
vbeAdder_1b	4	74	0,189189189
4gt10-v1_81	5	424	0,155660377
4gt13_92	5	190	0,157894737
4gt5_75	5	239	0,158995816
alu-v1_28	5	105	0,171428571
alu-v2_31	5	1295	0,152895753
decod24-v1_41	5	241	0,157676349
error_correctiond3_n5	5	278	0,176258993
q=5_s=2995_2qbf=09_1	5	3000	0,899
qec_en_n5	5	61	0,163934426
qec_sm_n5	5	61	0,163934426
quantum_volume_n5	5	411	0,124087591
simon_n6	5	92	0,152173913
4gt12-v0_87	6	711	0,157524613
4gt4-v0_72	6	740	0,152702703
alu-v2_30	6	1446	0,154218534
ex3_229	6	1153	0,151777971
graycode6_47	6	15	0,333333333
mod5adder_127	6	1577	0,151553583
q=6_s=2994_2qbf=08_1	6	3000	0,802
q=6_s=54_2qbf=022_1	6	60	0,233333333
qaoa_n6	6	528	0,102272727
sf_274	6	2221	0,151283206
xor5_254	6	17	0,294117647
4mod5-bdd_287	7	196	0,158163265
alu-bdd_288	7	240	0,158333333
C17_204	7	1341	0,152870992
ham7_104	7	922	0,161605206
majority_239	7	1754	0,152223489
q=7_s=2993_2qbf=08_1	7	3000	0,795333333
q=7_s=29993_2qbf=08_1	7	30000	0,799866667
dnn_n8	8	1904	0,100840336
f2_232	8	3456	0,151909722
hwb7_59	8	70093	0,152383262
q=8_s=2992_2qbf=01_1	8	3000	0,091666667
vqe_uccsd_n8	8	24136	0,22737819
q=9_s=19991_2qbf=08_1	9	20000	0,79645
q=9_s=2991_2qbf=01_1	9	3000	0,101
q=9_s=51_2qbf=012_1	9	60	0,116666667
adder_n10	10	328	0,198170732
q=10_s=990_2qbf=091_1	10	1000	0,899
sqn_258	10	29333	0,152013091
sym9_148	10	61824	0,152173913
shor_15	11	13588	0,131586694
16QBT_100CYC_QSE_1	16	1776	0,18018018
20QBT_45CYC_0D1_2D2_0	20	270	0,333333333